



ESFR-SIMPLE

Research and Innovation Action (RIA)

This project has received funding from the Euratom
research and innovation programme 2021-2025 under
Grant Agreement No 101059543

Start date : 2022-10-01 Duration : 48 Months

ESFR metallic fuel study: fuel and core designs

Authors : Dr. Konstantin MIKITYUK (PSI)

ESFR-SIMPLE - Contract Number: 101059543

Project officer: Cristina FERNANDEZ RAMOS

Document title	ESFR metallic fuel study: fuel and core designs
Author(s)	Dr. Konstantin MIKITYUK
Number of pages	42
Document type	Deliverable
Work Package	WP1
Document number	D1.1
Issued by	PSI
Date of completion	2023-09-08 13:47:23
Dissemination level	Public

Summary

Review and update of safety objectives. Select fuel type and make specification of the material properties including reference models for swelling, creep, fission gas release, etc. Design new fuel rod, new fuel assembly and new core

Approval

Date	By
2023-09-08 13:47:59	Dr. Konstantin MIKITYUK (PSI)
2023-09-08 13:52:06	Mr. Pierre SCIORA (CEA)

Disclaimer

The content of this report reflects only the author's view. The European Commission is not responsible for any use that may be made of the information it contains.

Document information

Grant Agreement	n°101059543
Project Title	European Sodium Fast Reactor – Safety by Innovative Monitoring, Power Level flexibility and Experimental research
Project Acronym	ESFR-SIMPLE
Project Coordinator	Pierre Sciora, CEA
Project Duration	1 October 2022 – 30 September 2026 (48 months)
Related Work Package	WP1. Advanced design and material studies for ESFR
Related Task(s)	Task 1.2. Metallic fuel option
Lead Organisation	PSI(14)
Contributing Partner(s)	ANL, HZDR(7), KIT(12), UCAM(2), EPFL(4), JRC(4)
Due Date	M6
Submission Date	
Dissemination level	PU

History

Date	Version	Submitted by	Reviewed by	Comments

Table of contents

1	Review of UK experience in metallic fuel for SFR (U-Mo).....	8
1.1	History of metallic fuel development in the United Kingdom	8
1.2	Irradiation performance of U-Mo metallic fuel in DFR	10
2	Review of US experience (U-Pu-Zr)	11
2.1	History of Metallic Fuel Development in the United States.....	11
2.2	Irradiation Performance of Metallic Fuel	15
2.3	Characteristics of Metallic Fuel in Off Normal and Transition Conditions	17
2.4	Recommendation for metallic-fuel SFR design.....	18
2.4.1	Pin design specifications	18
2.4.1.1	Smear density	18
2.4.1.2	Irradiation-induced swelling	18
2.4.1.3	Fuel-to-plenum volume ratio.....	19
2.4.2	Coolant and cladding temperatures.....	19
2.4.3	Irradiation performance	19
2.4.4	Inherent Safety.....	20
2.5	Recommendation for modelling thermal-physical properties of metallic fuel	20
2.5.1	Thermo-physical properties	20
2.5.1.1	Fuel thermal conductivity.....	20
2.5.1.2	Enthalpy, specific heat and melting temperatures	20
2.5.1.3	Phase transitions.....	20
2.5.1.4	Density and thermal expansion	20
2.5.2	Fuel swelling and fission gas release	20
2.5.3	Mechanical behavior and properties.....	21
2.5.4	Fuel constituent redistribution.....	21
2.5.5	Clad wastage	21
2.5.6	Clad properties and failure	22
3	ESFR-M fuel and core design.....	23
3.1	Overview of main recommendations for metallic-fuel SFR design	23
3.2	ESFR-M fuel and core design	24
3.2.1	Proposed design options.....	24
3.2.2	ESFR-M designing approach	26
3.2.3	ESFR-M core design specifications.....	28
3.3	Preliminary full core neutronic performance	32
4	Conclusions.....	38
5	Bibliography	39

List of figures

Figure 1: Fuel-Clad gaps for DFR metal fuel design variants [Crittenden 2019].	9
Figure 2: Swelling behavior of U-15.6 wt.% Mo as a function of temperature and burnup [Crittenden 2019].	11
Figure 3: Histogram of Mark-II Burnup in EBR-II.	13
Figure 4: Cladding Deformations Depending on Burnup.	14
Figure 5: Internal Pressure and Cladding Strain as Function of Burnup.	16
Figure 6: Cladding Diameter Strain and Fission Gas Release Rate with HT9 Cladding.	16
Figure 7: Subassembly designs of reference ESFR-SMART as well as three options proposed for ESFR-M.	25
Figure 8: ESFR radial core layout.	29
Figure 9: Axial layout of the ESFR-MOX and ESFR-M1 fuel sub-assemblies with a radial cut corresponding to the fissile region of each configuration.	30
Figure 10: ESFR-M1 core reactivity as a function of irradiation time and Pu content.	33
Figure 11: U (top) and Pu (bottom) vector masses evolution as a function of burnup for the ESFR-MOX and ESFR-M1 cores.	34
Figure 12: Pu-239 mass evolution as function of burnup for the ESFR-MOX and ESFR-M1 cores.	35
Figure 13: Core reactivity evolution as a function of burnup for both ESFR-M configurations.	36
Figure 14: Sodium void reactivity for different ESFR configurations.	37

List of tables

Table 1: Irradiation parameters of DFR metal fuel design variants.	8
Table 2: Fast Reactors Achieved Criticality.	12
Table 3: Comparison of Physics Data of Metallic and Oxide Fuels.	17
Table 4: Proposed designing approaches for the ESFR-M core with respect to the current ESFR-MOX design.	24
Table 4: Proposed designing approaches for the ESFR-M core with respect to the current ESFR-MOX design.	24
Table 5: Uranium and plutonium vectors used for fresh fuel composition.	27
Table 6: ESFR-MOX fuel mass at nominal conditions.	27
Table 7: U-Pu-Zr- fuel characteristics.	27
Table 8: Isotopic composition of U-Pu-Zr metallic fresh fuel (at cold and nominal operating conditions).	28
Table 9: ESFR-M axial dimensions: inner and outer fuel.	31
Table 10: ESFR-M axial dimensions: CSD and DSD.	31
Table 11: ESFR-M axial dimensions: corium discharge tube.	32
Table 12: ESFR-M axial dimensions: radial reflector.	32
Table 13: ESFR-M1 fissile fuel radial layout.	32

Summary

The ESFR-SIMPLE project includes among its main objectives the development and assessment of a new design of the 3600 MWth core based on a metallic fuel using as reference the ESFR system developed by the ESFR-SMART project. Then, Task 1.2 addresses the design of a version of the ESFR with a high-density fuel that might challenge the current oxide fuel design in terms of safety, fuel sustainability and waste minimization. The metallic fuel option is chosen because of significant operational experience, which is described in this report covering the UK and US experience and related activities.

As a result, recommendations are proposed for the design of a metallic-fueled version of the current ESFR core. In the frame of Task 1.2, the impact of the new fuel type on core design, performance and safety parameters, fuel cycle characteristics and behavior in selected accidents should be assessed and compared against the reference oxide option. Then, the main goal of this work is to develop an initial metallic-fueled ESFR design that serves as a base for subsequent analyses. Based on recommendations provided by ANL for the modelling and design of U-Pu-Zr metallic fuel, a preliminary version of the ESFR-M core is established. This proposal is accompanied by the assessment of the ESFR-M neutronic performance at BOL state and once-through burnup calculations, including a comparison with the reference case based on oxide fuel.

Thus, the work carried out in this report establishes the framework for subsequent subtasks within Task 1.2, where the ESFR-M design will be subject to an extended assessment in terms of neutronic performance, fuel behavior and transient analysis. Resulting from these analyses, an optimized version of the ESFR-M core design will be proposed.

Keywords

ESFR-M, metallic fuel, pre-design, core design

Abbreviations and acronyms

Acronym	Description
ANL	Argonne National Laboratory
BOL	Beginning of Life
CDF	Cumulative Damage Fraction
CDT	Corium Discharge Tube
CRBR	Clinch River Breeder Reactor
CSD	Control and Shutdown Devices
CW	Cold-Work
DFR	Dounreay Fast Reactor
DSD	Dedicated Shutdown Devices
EBR	Experimental Breeder Reactor
EOC	End of Cycle

EOL	End of Life
ESFR-M	European Sodium Fast Reactor with Metallic fuel
ESFR-SMART	European Sodium Fast Reactor – Safety Measures Assessment and Research Tools
FFTF	Fast Flux Test Facility
IF	Inner fuel
OF	Outer fuel
MOX	Mixed oxide fuel
SA	Solution Annealing
FCCI	Fuel and Cladding Chemical Interaction
SFR	Sodium Fast Reactor
ULOF	Unprotected Loss Of Flow
ULOHS	Unprotected Loss Of Heat Sink
UTOP	Unprotected Transient Overpower

Introduction

Metallic fuel is the reference fuel in the USA for Sodium-cooled Fast Reactors (SFR), according to a vast operational experience as well as many research activities. On the other hand, oxide fuel has been the selected option for several European countries in the frame of previous research activities that led to the design of oxide-fueled SFR systems [Fiorini 2011, Mikityuk 2017]. Then, the ESFR-SIMPLE, as the latest European iteration on the SFR design, includes among its main goals the development and assessment of a modified version of the European Sodium Fast Reactor (ESFR) based on a metallic fuel.

The metal and oxide fuel types differ in their properties, such as density or thermal conductivity, and provide the reactor with unique set of responses to operational transients. The ESFR-SIMPLE project aims to deliver a thorough comparison concerning the benefits and limitations of these two fuel types for the same reactor design. In the frame of Task 1.2, this comparison will cover a wide variety of parameters, involving neutronic performance, fuel behavior, and response to different unprotected transient sequences.

Nonetheless, the proposal of a core design is required as first step in order to provide a framework for subsequent analyses. Then, with the aim of selecting main designing parameters, a detailed review of past experience should be carried out to benefit the ESFR with metallic fuel (ESFR-M) design from related recommendations. In this work, a detailed review of both UK and US experience regarding the use of metallic fuel is presented in Sections 1 and 2, respectively, with particular emphasis on the irradiation performance of selected metallic fuels.

Based on the existing irradiation data from experimental facilities, a variety of recommendations is provided for the design of a metallic-fueled SFR design. Selected parameters are considered to be licensable so that they are taken into account for the design of the ESFR-M, which is described in Section 3. The designing approach aims to maintain the current oxide-fueled ESFR core specifications while the fuel pin is modified by a sodium-bonded U-Pu-10Zr fuel pin. Smear density and fuel-to-plenum volume ratio requirements are considered through the designing phase, leading to different ESFR-M configurations. A sensitivity analysis to the plutonium content is also carried out for exploring the performance of these configurations with reduced plutonium content. A preliminary set of neutronic parameters is evaluated for the most promising configurations and compared to the reference oxide option.

As a result, an initial ESFR-M configuration is proposed to be applied in subsequent analyses, with other alternative options to be considered depending on the feedback provided by further safety analyses.

1 Review of UK experience in metallic fuel for SFR (U-Mo)

A. Dubey, University of Cambridge (UCAM)

1.1 History of metallic fuel development in the United Kingdom

The UK experience in metal fuels for SFRs stems from the investigations carried out at the Dounreay Fast Reactor (DFR) [Crittenden 2019]. The DFR was designed with 60 MW(th) and 12 MW(e) capacities and 70/30 Na-K alloy coolant. Metallic fuel (U alloy) rods (or elements) were initially chosen as drivers of the DFR core to demonstrate a high breeding potential and utilize pre-existing knowledge of metallic fuel cycle from Magnox reactors. Variants of U-Cr and U-Mo alloys were utilized as annular fuel slugs, which were restrained by Vanadium / Niobium cladding at the inner and outer surfaces. Table 1 specifies the DFR metal fuel design variants and their associated irradiation parameters. The first fuel element design was 'MK II Standard'. Subsequent variants were designed to increase the maximum allowable burnup. The final variants (MK III series) reached a peak burnup of 3.65 at.%.

Table 1: Irradiation parameters of DFR metal fuel design variants

Design	Fuel composition	Clad composition	Burnup levels	DFR Power level
MK II Standard	U-0.5 at.% Cr	V (in), Nb (out)	0.1 at.%	11 MW(th)
MK IIB	U-20 at.% Mo	Nb (in / out)	0.81 at.%	15-30 MW(th)
MK IIC	U-20 at.% Mo	Nb (in / out)	0.81 at.%	15-30 MW(th)
MK IIIA	U-20 / 15.6 at.% Mo	Nb (in / out)	2.5 at.%	60 MW(th)
MK IIIB	U-20 / 15.6 at.% Mo	Nb (in / out)	3 at.%	60 MW(th)
MK IIIC	U-20 / 15.6 at.% Mo	Nb (in / out)	3 at.%	60 MW(th)

The first variant (MK II) utilized 45% enriched U and Cr (U-0.5 at.% Cr) alloy as fuel with inner and outer diameters of 6.35 mm and 19.05 mm, respectively [Crittenden 2019]. The fuel-clad gaps were filled with Na, and vents were provided in the top plug to enable escape of gaseous fission products outside the fuel elements. The U-0.5 at.% Cr alloy failed to exhibit dimensional stability under irradiation¹. Accommodation of fuel swelling via axial extrusion (strong-clad-weak-fuel approach) was found to be impractical since stresses induced by FCMI led to rapid clad creep at operating temperatures. Additionally, severe hydrogen embrittlement of clad tubes (Vanadium / Niobium) was noticed². Studies showed Vanadium to be more susceptible to hydrogen embrittlement compared to Niobium.

Consequently, the MK IIB / C elements were designed with U-20 at.% Mo alloy and Niobium inner / outer cladding to improve resistance against fuel swelling and hydrogen embrittlement, respectively. An extensive coolant clean-up campaign was also undertaken to remove high concentrations of oxides and hydrides from the primary circuit. The elements were irradiated under intermediate power (16-30 MW(th)) to burnup levels of 0.1-0.57 at.% (standard) and 0.24-0.81 at.% (pilot) [Crittenden 2019]. The performance of these elements did not inspire confidence in their ability to sustain 0.5 at.% burnup at full power. The U-20 at.% Mo alloy

¹ At 0.1 at.% burnup, the fuel element exhibited surface wrinkling, increase in outer diameter of 0.18 mm, contraction of inner hole, outer clad distention, and strong fuel-clad mechanical interaction (FCMI) at the inner surface.

² Clad failure occurred during fuel handling operations at temperatures below 100-200°C. This occurred usually after fuel was removed from the element.

exhibited lower thermal conductivity compared to U-0.5 at.% Cr, which was hypothesized to result in fuel temperatures as high as 900°C at full power. At such temperatures, the swelling resistance of U-20 at.% Mo alloy was known to be grossly impaired. Therefore, rapid clad distension and failure were anticipated at full power.

The MK III fuel elements were designed to overcome the above limitations. The MK III design variants (MK IIIA / B) contained fuel-clad gaps of 76 μm and 760 μm at the inner and outer fuel surfaces, respectively (Figure 1). An enrichment of 75% was utilized to compensate the reduction in fuel volume. A two-zone core was introduced with MK IIIB and MK IIIA (thicker fuel annulus than that of MK IIIB) elements arranged in the inner and outer zones, respectively. Appreciating that a large fuel-clad gap width could lead to lateral fuel movement within the element, anti-bow washers (Niobium discs) were introduced between fuel slugs to maintain the inner and outer clad concentricity. The elements were irradiated at full power (60 MW(th)) to a maximum burnup of 1.06 at.% in the first DFR run. Encouraging findings from post-irradiation examination led to progressive increase in burnup levels. Observations of localized fuel melting near anti-bow washers led to the introduction of triangular washers that guaranteed optimal bond flow³. Several fuel elements attained burnup levels above 3 at.% (3.65 at.% peak burnup) [Crittenden 2019]. Additional changes were subsequently introduced to gain reactivity increments, such as reduction in Molybdenum content from 20% to 15.6%, introduction of MK IIIC elements (annulus thickness of 2.95 mm) in place of MK IIIB elements (annulus thickness of 2.74 mm), and replacement of axial breeders (natural U) with stainless steel reflectors.

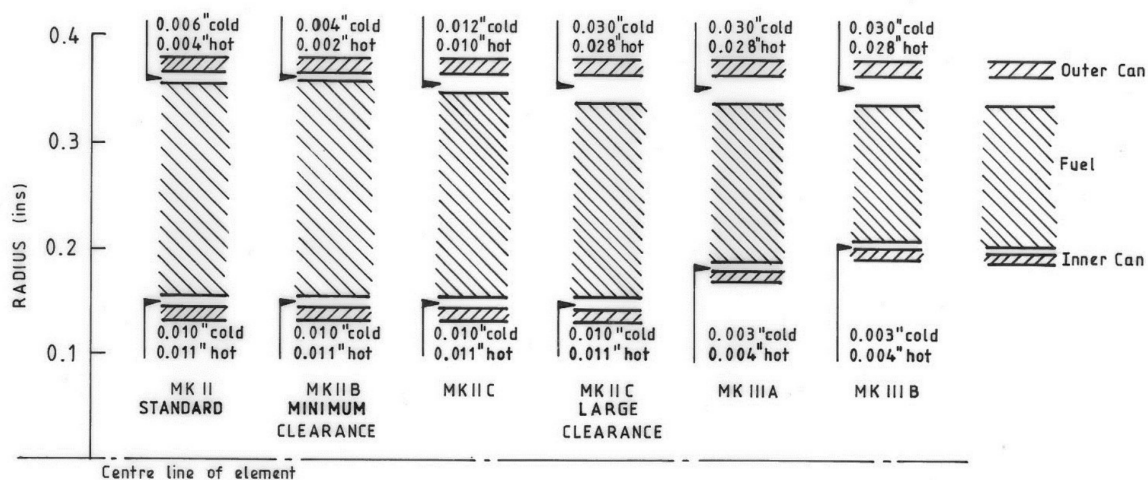


Figure 1: Fuel-Clad gaps for DFR metal fuel design variants [Crittenden 2019].

A deterioration in MK III fuel performance was recorded during DFR runs 56-60, which involved an extended shutdown period aimed at modification of the radial breeder (September 1965-February 1966) [Crittenden 2019]. Clad distension of 0.36 mm (2.8 at.% burnup) appeared at 2.8 at.% burnup, which indicated that further irradiation could result in difficulties in fuel element discharge. A provisional burnup limit of 2.5 at.% was assigned to standard fuel elements

³ Localized fuel melting occurred in original MK III elements irradiated to burnup levels higher than 0.7 at.%. This was confirmed based on the presence of metallic globules (~0.5 mm in diameter) at the fuel surface in proximity with Niobium washers. Metallographic examination revealed the existence of gross local swelling near Niobium washers characterized by hollow spherical globules at the fuel surface. Results of out-of-pile tests indicated the possibility of large gas bubbles anchored near Niobium washers, which could have impeded heat transfer and initiated fuel melting. The problem was ameliorated by introducing triangular Niobium washers, which would increase bond flow and sweep away any gas bubbles formed. No further instances of localized globule extension were observed subsequently.

installed in fixed locations. The fuel elements installed in control rod carriers, which could be removed from the core as a unit, were irradiated to higher burnup.

Further deterioration was observed after a second prolonged shutdown following the discovery of a primary circuit leak in July 1967 [Crittenden 2019]. Breakaway swelling (initiation of rapid fuel swelling expected typically after 2 at.% burnup) was now observed at 0.5-1.0 at.% burnup. Ten fuel elements (3.2-3.4 at.% burnup) were found jammed in control rod carriers after run 73. The reason for deterioration was derived from the results of metallographic analysis, which indicated an intermittent presence of abnormally high fuel temperatures. It was inferred that such intermittent temperature spikes were caused by the presence of bubbles entrained from the primary circuit in the Na bond. Fuel performance could not be restored back to pre-leak levels after DFR run 60. Final burnup limits endorsed for MK IIIA and MK IIIC fuel elements were 2.5 at.% and 3 at.%, respectively.

Post-irradiation examination of MK III fuel elements revealed that despite volume increases of the order of 30-40 vol.% prior to fuel-clad contact, FCMI stresses developed rapidly (circa 700 MPa), threatening clad rupture. High sensitivity of fuel performance towards temperature abnormalities was observed with deviations of circa 10°C resulting in significant performance deterioration. It was concluded that the endorsed burnup limits could be increased further by utilizing a stronger or thicker clad material or by reducing the fuel temperature; however, a burnup limit in excess of 5 at.% would be unlikely. An additional limitation of MK III type fuel elements was the upper limit of the coolant outlet temperature (500°C), which was essential to maintain Niobium corrosion resistance (unless high coolant purity could be guaranteed). Furthermore, the vented can concept led to an inability to detect fuel element failure in-situ using fission gas or delayed neutron monitoring systems. Owing to these limitations, efforts were diverted towards cermet, carbide, and oxide fuels in search of a commercially viable SFR fuel design [Crittenden 2019]. Although a transition from U-Mo to U-Pu based alloy variants was originally planned, it was not initiated. Therefore, the UK did not acquire experience in the behavior, manufacturing or reprocessing of U-Pu alloy based SFR fuels.

A noteworthy point regarding the history of metal fuel development in the UK is the absence of transient test records [Crittenden 2019]. There appears to have been no in-pile transient / off-normal testing of metal fuels in the DFR.

1.2 Irradiation performance of U-Mo metallic fuel in DFR

Prominent irradiation-induced swelling was observed in all metallic fuel element variants irradiated in DFR. Fuel-clad gap width played a crucial role in irradiation performance⁴ (Figure 1). U-Mo alloys exhibited improved swelling resistance over U-Cr alloys⁵ [Crittenden 2019]. Three distinct swelling rates were observed up to 1.4 at.% burnup (U-15.6 at.% Mo, Figure 2). These were 6 vol.%, 2.5 vol.%, and 10 vol.% per 1 at.% burnup for fuel center temperatures of ~600°C, lower than 500°C, and 500-600°C, respectively. The increased rate of swelling in the 500-600°C range was caused by the breakdown of the gamma phase. Swelling remained a function of fuel temperature, burnup, and Molybdenum content until 2 at.%. The U-20 at.% Mo alloy performed slightly better in comparison with the U-15.6 at.% Mo alloy in terms of swelling resistance above 600°C. Above 2 at.%, fuel slugs were split longitudinally, which led to rapid swelling up to 30-35 vol.%, resulting in fuel practically occupying the can completely at approximately 2.5 at.%. Above 2.5 at.%, swelling was restrained by the can in both radial

⁴ Gap closure in the MK II B/C and MK III series occurred at burnup levels of 0.3 at.% and up to 1 at.%, respectively, because of the differences in gap widths.

⁵ Increase in outer diameter of 0.18 mm was observed at 0.4 at.% burnup in uncracked fuel pieces of U-20 at.% Mo. An equal increase in outer diameter was attained at 0.1 at.% burnup in case of U-0.5 at.% Cr. Above 0.25 at.% burnup, increases in outer diameter of U-20 at.% Mo were primarily due to cracking.

and axial directions (MK III series). Subsequently, clad yielding initiated as a function of local stresses and clad temperature.

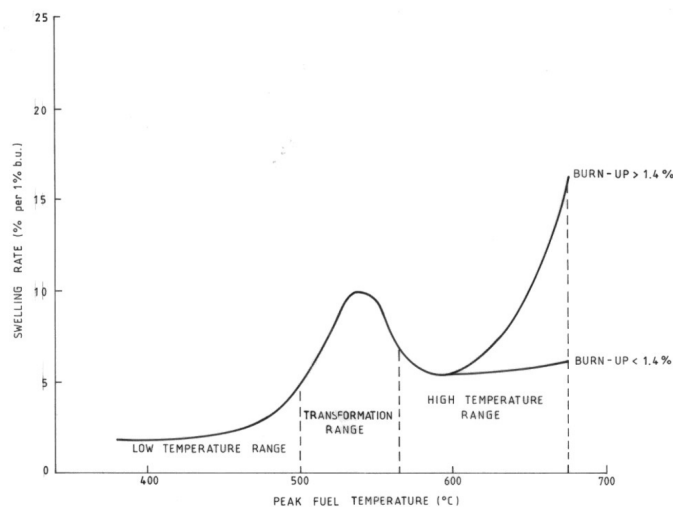


Figure 2: Swelling behavior of U-15.6 wt.% Mo as a function of temperature and burnup [Crittenden 2019].

Inter-connected porosities were observed at the grain boundaries as well as within grains, indicating paths for release of gaseous fission products at volume increases above 25%; however, a substantial fraction of fission gases still remained trapped within the fuel microstructure. Note that the vented fuel element design led to reduced fission-gas pressure.

Corrosion and hydrogen embrittlement remained key concerns throughout the DFR metal fuel development. Oxide films (0.025-0.05 mm thickness) were observed on the surfaces and cracks of U-20 at.% Mo alloy at 0.81 at.% burnup. High Niobium corrosion rates of up to 1.1 mm/100 days were observed in experimental fuel elements with maximum clad temperature of 520°C, resulting in complete clad corrosion near the bottom of fuel elements. The probability of embrittlement-related clad fracture was found to increase when coolant impurity levels were high⁶. These results indicated a need for reducing coolant outlet temperatures and coolant impurity levels to preserve the Niobium cladding. Upon maintaining the Niobium outer clad temperature beneath 500°C, corrosion losses reduced to 0.075 mm above 3 at.% burnup. The inner clad (500°C) exhibited corrosion rates of 0.075-0.2 mm/100 days. Upon decreasing oxygen content in the Na-K coolant from 12 ppm to 5 ppm, the corrosion rate of the inner clad (500°C) reduced to 0.075 mm/100 days, indicating strong corrosion resistance under the given temperature and coolant impurity limits.

2 Review of US experience (U-Pu-Zr)

2.1 History of Metallic Fuel Development in the United States

T. K. Kim, Argonne National Laboratory (ANL)

A list of the fast reactors that have been built, achieved criticality, and operated is provided in Table 2. Metallic fuel was selected for the early fast reactors in the United States because of ease of fabrication, high thermal conductivity, high breeding ratio with harder neutron

⁶ Embrittlement-induced clad failure occurred during fuel handling operations once fuel slugs were removed from within the clad tubes.

spectrum, compact core size with higher fuel density, and compatibility with a liquid metal coolant.

Table 2: Fast Reactors Achieved Criticality

Reactor	Country	MWth	First critical	Fuel form
Clementine	USA	0.025	1946	Metal
EBR 1	USA	1.4	1951	Metal
BR-10	Russia	8	1958	Nitride
DFR	UK	60	1959	Metal
LAMPRE	USA	1.0	1961	Molten
EBR II	USA	62.5	1961	Metal
Fermi I	USA	200	1963	Metal
RAPSODIE	France	40	1967	Oxide
BOR-60	Russia	55	1968	Oxide
SEFOR	USA	20	1969	Oxide
KNK II	Germany	58	1969	Oxide
BN 350	Kazakhstan	750	1972	Oxide
PHENIX	France	563	1973	Oxide
PFR	UK	650	1974	Oxide
Joyo	Japan	140	1977	Oxide
FFTF	USA	400	1980	Oxide
BN 600	Russia	1470	1980	Oxide
S-PHENIX	France	3000	1985	Oxide
FBTR	India	40	1985	Carbide
MONJU	Japan	714	1994	Oxide
CEFR	China	65	2010	Oxide
BN 800	Russia	2100	2014	Oxide

Experimental Breeder Reactor I (EBR-I) was initially fueled with unalloyed uranium metallic fuel, U-Zr, and Pu-Al binary alloy fuels. The Fermi I reactor was fueled with U-Mo binary alloy fuel. Experimental Breeder Reactor II (EBR-II) was started up with a fuel alloy of 95% uranium and 5% fissium (Simply U-5Fs, Mark-I, and Mark-II designs), but the fuel was converted to U-Zr (Mark-III design). It is noted that the EBR-II fuel was recycled through melt-refining and injection casting fabrication [Stevenson 1987] in the early stages of the reactor's existence, and the noble metal fission products, so-called fissium (Fs), were reloaded back along with the recovered uranium. The fissium consists of about 2.5% Molybdenum, 1.9% ruthenium, 0.3% rhodium, 0.2% palladium, 0.1% zirconium, and 0.01% niobium [Hofman 1997].

As shown in Table 2, however, the fast reactor fuel form was changed to an oxide fuel starting in the late 1960s because it was hard to achieve a higher burnup with metallic fuels. The early irradiation experience of metallic fuels in the EBR-II shows that the burnup of the metallic fuels (Mark-I and Mark-IA) is limited by ~3 at.% depending on the fuel compositions because the metallic fuel pins resulted in a cladding breach by the fuel swelling and internal pressure driven by gaseous fission products. Additionally, due to the technological progress of oxide fuel fabrication in commercial light water reactor sectors and the reprocessing of oxide fuels [Walters 1984, Leggett 1993], oxide fuel was attractive in the late 1960s among countries that later started the development of fast reactor technologies.

In the United States, the oxide fuel has been considered and used in Fast Flux Test Facility (FFTF) and Clinch River Breeder Reactor (CRBR), and EBR-II's mission was changed to support the irradiation test of mixed oxide fuel [Hofman 1994, Hofman 1997, Walters 1999]. However, the development of metallic fuel for higher burnup continued, and its burnup capability was drastically improved through discoveries and irradiation experience with low-smeared density fuels in the 1970s [Walters 1984, Seidel 1987, Hofman 1997]. The key discovery was to provide sufficient free space initially to accommodate fuel swelling and fission gas: i.e., a fuel-to-cladding gap filled with sodium bond and a larger space of gas plenum. Later, low-swelling advanced cladding materials, such as D9 and H9, were developed.

The Mark-II metallic fuel pin of EBR-II was designed with 75% smeared fuel density, while the original Mark-I fuel incorporated 85% smeared fuel density. The achieved burnup was increased, and the Mark-II fuel pin design proved to be capable of reliable operation to the burnup of 10 at. % [Einziger 1980, Olson 1980]. Figure 3 shows the irradiation experience of Mark-II fuel pins in EBR-II. Over 40,000 Mark-II fuel pins had been irradiated by the early 1980s, and some fuel pins reached 18.5 at.% burnup [Walters 1987].

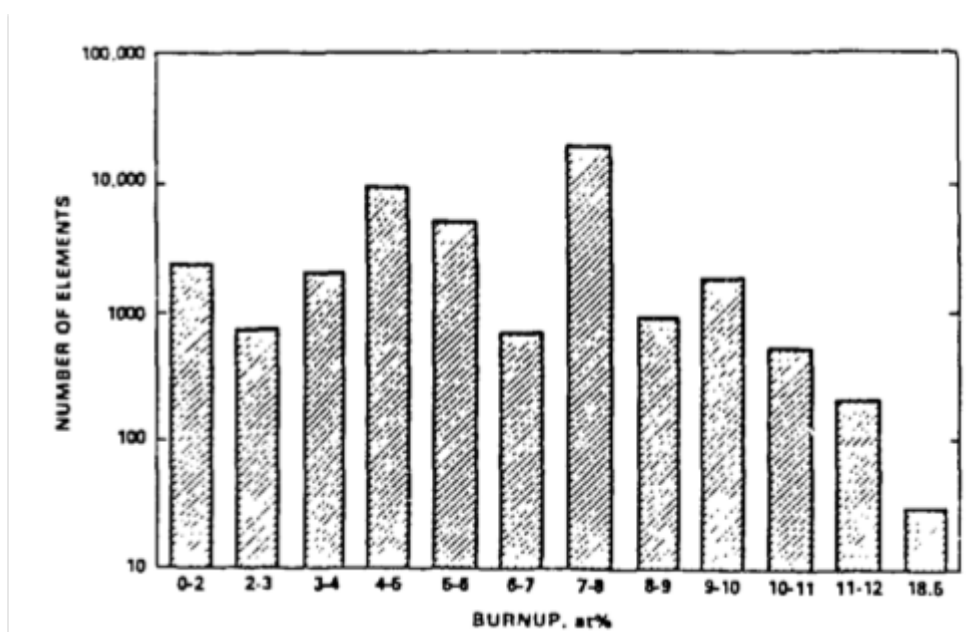


Figure 3: Histogram of Mark-II Burnup in EBR-II

Metallic fuels with various alloy elements were investigated for the EBR-II core conversion. Several alloy elements (Zr, Mo, Al, Cr, etc.) were considered to raise the solidus temperature, and Zr seemed promising due to its reduction of fuel/cladding inter-diffusion and favorable early irradiation testing results [Leggett 1993, Walters 1980]. The driver fuels of the EBR-II were converted to U-Zr (Mark-III design) [Einziger 1980, Lahm 1993, Walters 1984] from U-5Fs (Mark-II) in the 1980s. In particular, it was observed that the solidus temperature of metal fuel was improved with at least 10 wt% zirconium in the fuel alloy, and based on the discovery, the present metallic fuels are usually 10 wt% zirconium alloys.

Various cladding materials have been developed. Figure 4 shows the peak diametral strain of several cladding materials such as SS-304, SS-316, D9, and HT9 fabricated by solution annealing (SA) or cold-work (CW) [Hofman et al. 1997]. Type 304 or 316 stainless steel cladding was selected in the early EBR-II fuels. However, due to large irradiation-induced deformation, the stainless-steel cladding was replaced with austenitic D9 cladding and later, ferritic–martensitic HT9 cladding was developed in Mark-IV fuels. HT9 has been selected as the cladding material in the ALMR design because of the attractive irradiation performance till

a higher burnup. However, HT9 has a relatively higher penetration rate of lanthanides into the cladding at a lower temperature compared to Type 316 stainless steel. Thus, operation conditions (in particular, the temperature at the fuel and cladding interface) of fast reactors with HT9 cladding have been determined to mitigate fuel and cladding chemical interaction (FCCI).

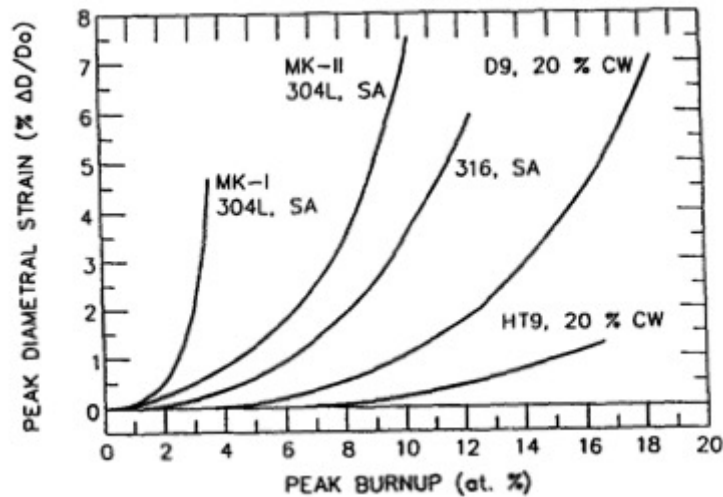


Figure 4: Cladding Deformations Depending on Burnup

The U.S. fast reactor program was reassessed in the 1980s: the Clinch River Breeder Reactor (CRBR) program was canceled, and the Integral Fast Reactor (IFR) program was proposed in 1983 [Till 1988, Chang 1989] to provide non-proliferation and improved, inherent reactor safety characteristics through the use of metallic fuel, which provided improved feedback characteristics, good fuel/coolant compatibility in the case of cladding breach, beneficial transient overpower behavior, and high burnup capability, as were proven in the EBR-II fuel tests.

To achieve a closed fuel cycle, the use of a significant amount of plutonium in a fast reactor was expected, and the development of U-Pu-Zr ternary fuel (Mark-V/VA) was continued in EBR-II based on the successful fuel conversion experience to U-Zr fuels (Mark-III and Mark-IV) from U-Fs fuels (Mark-II). The addition of Pu to form the ternary U-Pu-Zr alloy did not change the mechanisms that control fuel element lifetime [Porter 1986], although the Pu addition and other characteristics of higher-burnup fuel had an impact on the fuel/cladding inter-diffusion and fuel constituent migration, etc. [Kim 2006]. In 1984, the Experimental Fuels Laboratory was established to fabricate plutonium-bearing ternary fuel, leading to the fabrication of a total of 16,811 U-Zr and 660 U-Pu-Zr fuel pins, which were irradiated in EBR-II until the reactor was permanently shut down in 1994. Even though the experimental database obtained from the irradiation information in EBR-II was mainly made up of non-ternary U-Pu-Zr fuel, it was sufficient to support the initial review of the safety case to convert the EBR-II driver core to U-Pu-Zr ternary fuel [Briggs 1995].

Overall, more than 130,000 metallic fuel rods were fabricated and irradiated in EBR-II, and the FFTF and the metallic fuels were qualified to 10 at.% burnup, demonstrated to 20 at.% burnup with HT9 cladding with Pu content up to 31%. Detailed irradiation information is summarized by [Crawford et al, 2007].

Since EBR-II and FFTF were permanently shut down in the 1990s, there have been no major irradiation tests of the metallic fuels in the U.S., but the fast reactor fuel development programs were continued under the Advanced Fuel Cycle Initiative (AFCI) [Hilton 2006], the Global

Nuclear Energy Partnership (GNEP), and the Fuel Cycle Research and Development (FCRD) programs of the Nuclear Office of U.S. Department of Energy. Since there are no fast neutron flux facilities for the irradiation test, the recent fast reactor fuel development programs of the U.S. emphasize modeling and simulations [Konings 2012, Braase 2010] to address the technical issues and/or challenges related to the advanced fast reactor fuels, which includes a significant increase in burnup and performance over the current technologies, near zero-loss fuel fabrication processes containing minor actinides, innovative fuel concept that is tolerant to severe accidents, etc.

One of the significant efforts that are part of the FCRD program is the development of the innovative metallic fuel [Wright 2010, Braase 2010], which is being pursued jointly by Argonne National Laboratory and Idaho National Laboratory aiming to develop and demonstrate the feasibility of a metallic fuel form capable of reliable performance up to 30 – 40 at.% burnup and fabrication methods that reduce process losses less than 1%. The innovations in the ultra-long burnup metallic fuel include a further decrease in smeared fuel density, coating or liner on the cladding inner surface [Sridharan 2012], venting of the gaseous fission products to the sodium coolant [Kim 2010], consideration of a U-Mo based alloy fuel system, targeted fuel alloy additions to reduce fuel-cladding chemical interaction, and an advanced fabrication method that includes consideration of annular fuel.

2.2 Irradiation Performance of Metallic Fuel

T. K. Kim, Argonne National Laboratory (ANL)

One of the important phenomena of metallic fuel during fast neutron irradiation is irradiation-induced swelling. Large swelling occurs at a low burnup (1 – 2 at.%) in a typical operating temperature range of the sodium-cooled fast reactors (SFRs). The swelling is due to extensive fission-gas porosity [Chang 2007, Hofman 1997]. This high rate of swelling creates stresses in the peripheral fuel large enough to result in a cladding breach that was observed in the early EBR-II metallic fuels (in particular, Mark-I fuels).

Through the continuous irradiation of the metallic fuels in EBR-II, it was observed that the fission gas porosity tends to be interconnected at ~30% swelling, and gaseous fission products leak to a gas plenum through the porosity connections [Blake 1961, Beck 1968]. Thus, sufficient free space between the fuel slug and cladding for accommodating fuel swelling and a large gas plenum for accommodating the gaseous fission products allow a higher burnup without a cladding breach. Figure 5 shows pressures inside cladding and cladding strain as a function of burnup [Blake 1961]. It is provided to show trends of strain and pressure as a function of burnup, but should not be used to assess clad strain as this analysis was not accounting for Fuel Clad Mechanical Interaction. Both sufficient free space between the fuel slug and cladding with a low smeared density and the large gas plenum mitigate internal pressure and cladding strain up to the higher burnup.

In order to determine the effective smeared density, the metallic fuels with HT9 cladding were irradiated varying the smeared fuel density [Tsai 1991]. Figure 6 shows the cladding diameter increase and fission gas release fraction of the ternary metallic fuel at 12.5 at.% burnup. The fission gas release rate maintains ~85% up to the smeared density of 75% and decreases as the smeared density increases further. After these observations, the smeared fuel density of a metallic fuel was chosen to be approximately 75% from Mark-II fuel, which allows approximately 30% swelling. The gas plenum volume to accommodate the released fission gas was decided to be comparable to or larger than the fuel volume (i.e., plenum-to-fuel length ratio within the cladding is one or higher). The 75% smeared density allows ~14% increase in

the fuel radius until the metal slug contacts the cladding inner wall and the metallic fuel grows axially by 2 – 8% depending on the fuel composition [Hofman 1997, Seidel 1990]. Based on the irradiation experience and observations, the smeared density of a present metallic fuel with HT9 cladding is designed to be 75%.

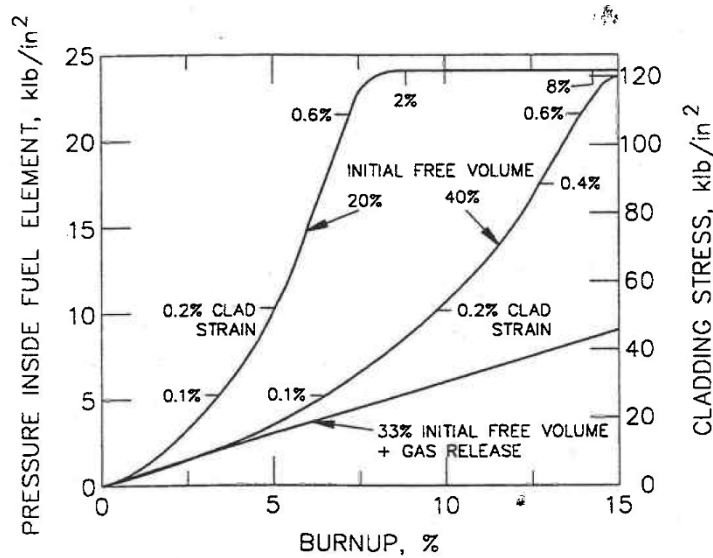


Figure 5: Internal Pressure and Cladding Strain as Function of Burnup

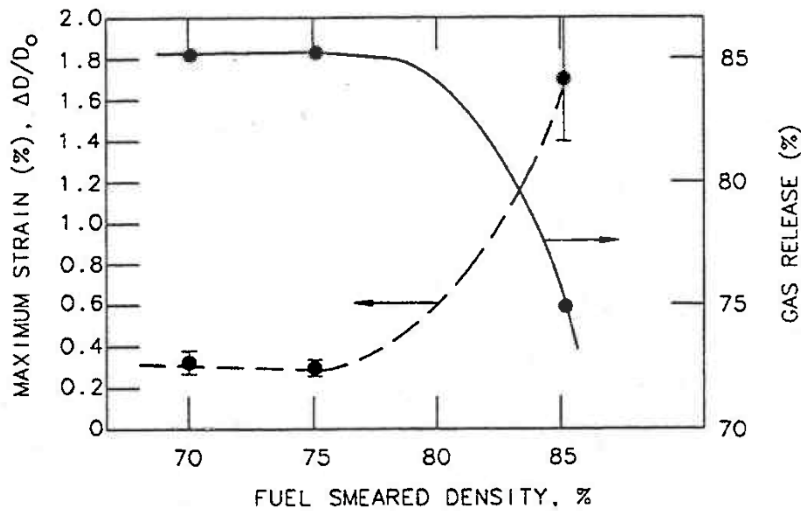


Figure 6: Cladding Diameter Strain and Fission Gas Release Rate with HT9 Cladding

FCCI is a complex problem including constituent redistribution. In high plutonium ternary fuel, constituent redistribution occurs in the early stage of irradiation, and radial fuel zones are formed. The constituent migration is driven primarily by a temperature gradient, and hence it is predominantly radial redistribution. Zirconium tends to migrate to the center and the periphery, and uranium migrates in the opposite direction. Plutonium on the other hand tends to remain in same location. This is fortuitous and tends to help the performance issues in that Zr moves to the center raising the solidus temperature at peak temperature region and to the periphery helping the fuel-cladding compatibility. [Hofman 1997]

2.3 Characteristics of Metallic Fuel in Off Normal and Transition Conditions

T. K. Kim, Argonne National Laboratory (ANL)

Major physics data of the metallic and oxide fuels in the typical environment of SFRs are compared in Table 3. Compared to oxide fuel, metallic fuel has superior thermal conductivity but a much lower melting temperature. As a result, the fuel centerline temperature to the fuel melting temperature of the metallic fuel is comparable to the oxide fuel, which results in a comparable safety feature in normal operating conditions. However, metallic fuel has excellent inherent safety features in off-normal and severe accident conditions.

Table 3: Comparison of Physics Data of Metallic and Oxide Fuels

Fresh Fuel Properties	Metal (U-Pu-10Zr)	Oxide (UO ₂ -PuO ₂)
HM Density, g/cm ³	14.1	9.3
Melting Temperature, K	1350	3000
Thermal Conductivity, W/cm-K	0.16	0.023
Centerline Temperature at 40 kW/m, K	1060	2360
Centerline-to-melting temperature	0.8	0.8

The metallic fuels were irradiated under off-normal and transition conditions in the EBR-II and Transient Reactor Test Facility (TREAT) [Chang 2007, Seidel 1986(b)]. First, the Run-beyond-cladding-breach (RBCB) tests have been conducted using U-Fs, U-Zr, and U-Pu-Zr fuels with various cladding materials [Bette 1990]. In the RBCB test, metallic fuels having defective cladding (i.e., hole) were irradiated more than 10 at.% burnup. Because of the excellent compatibility between the fuel slug and sodium coolant, there were no reaction products; the fuel loss was practically zero; and there was no indication of breach site enlargement to high burnup. However, the breach site was enlarged in the oxide fuel. This observation indicates that the defect in metal fuel cladding is not enlarged or propagated by neighboring fuel pins.

Various tests were performed in the TREAT to assess the transient-overpower margin to fuel failure, pre-failure axial fuel expansion, and post-failure fuel and coolant behavior with various combinations of fuel compositions and claddings [Hofman 1997, Bauer 1990]. The results consistently showed that the metallic fuel failure threshold is a factor of four higher than nominal power under the relatively fast transient-overpower conditions used in the tests. The data from these tests and from a large number of previous metallic fuel transient tests in TREAT were used to develop and validate models of fuel behavior under transient overpower conditions [Sofu 1996, Miles 1988].

In 1986, two landmark passive safety tests of unprotected loss of flow (ULOF) and unprotected loss of heat sink (ULOHS) were conducted in EBR-II as part of the IFR safety programs [Fistedis 1987]. The ULOF event was initiated by the station blackout of EBR-II and assumed that all active safety systems and operator actions had failed. As the power was lost, the coolant flow was reduced rapidly while the reactor was at its full power, which caused the reactor coolant outlet temperature to rise very rapidly (about 200°C in 30 seconds) and the neutron leakage rate to increase due to the thermal expansion of the core components. The negative reactivity feedback shut down the reactor and the natural heat loss mechanism stopped the increase in coolant temperature below the boiling temperature.

Following the ULOF test, the ULOHS test was conducted on the same day. The loss-of-heat sink was initiated by the shutdown of the intermediate pump, which isolated the primary system, while the primary pump was functioning to remove the heat from the core to the primary tank. The intermediate loop flow was reduced to zero, which disabled the normal heat sink in the balance of the plant. The core heat was dumped into the entire inventory of the primary sodium, which raises the core inlet temperature. Similarly, the increase in the reactor inlet temperature enhanced the neutron leakage rate and induced negative reactivity feedback. Finally, the reactor power was reduced, and the reactor outlet temperature was reduced accordingly.

The tests successfully demonstrated the ability of the pool-type SFR with metallic fuels to withstand potential severe accidents (ULOF and ULOHS) because the unique combination of the high heat conductivity of metallic fuel and the thermal inertia of the large sodium pool can shut down the reactor without depending on human intervention or the operation of active safety and engineered components.

2.4 Recommendation for metallic-fuel SFR design

N. Stauff and T. K. Kim, Argonne National Laboratory (ANL)

The objective of this section is to summarize the present practices utilized for designing metallic-fueled SFRs. This document focuses on sodium-bonded U-Pu-10Zr fuel pins with HT9 cladding material. It is noted that the low swelling HT9 is preferred as a cladding material for a higher burnup rather than austenitic stainless cladding materials. Following these recommendations should ensure satisfactory (but maybe not optimum) performance in terms of neutronics, thermo-mechanics and safety. These conventional design parameters are considered to be licensable in the U.S. using the existing irradiation data from EBR-II and FFTF [Crawford 2007, Hofman 1997, Chang 2007].

2.4.1 Pin design specifications

The metallic fuel is recommended with 10w% of Zr for raising the solidus temperature and improving the chemical stability. Past successful irradiation experiments had Pu fraction limited to < 31 w% [Chang 2007], pin outer cladding diameter from 0.584 cm to 0.94 cm [Crawford 2007] and HT9 cladding thickness of 0.038-0.051 cm. Similar parameters would be preferred to remain within the range of qualified pin designs. However, thicker fuel pin should be acceptable as long as the smeared density and fuel to plenum ratios are maintained.

2.4.1.1 Smeared density

A smeared density⁷ around 75vol% is recommended for the fresh fuel, and is achieved with a large initial gap that is filled with liquid sodium (with 1-2 cm of excess sodium filled above the fuel slug). Such smeared density is required to keep sufficient room radially for the fuel to swell before it reaches the cladding. Formation of interconnected open porosity structure prior to hard contact between fuel and cladding ensures that solid fission product swelling can be accommodated with low fuel clad mechanical interaction [Hofman 1997]. The smeared density can further be reduced to achieve higher burnups with low clad straining. The most successful highest burnup pins that were irradiated in EBR-II has 72.5% smear density.

2.4.1.2 Irradiation-induced swelling

Because of quick fuel swelling radially and axially at beginning of life (within ~1at% burnup [Hofman 1997]), the expanded fuel needs to be modeled for neutronics analyses. The U-Pu-10Zr fuel grows ~5% axially by irradiation-induced swelling, the fuel slug swells till contacting

⁷ Smeared density is calculated as the metal slug area over the inner cladding area.

the cladding inner wall, and the sodium bond fills the 70-85%vol of the porosity in the fuel slug and the remaining relocates above the fuel (in the gas plenum).

2.4.1.3 Fuel-to-plenum volume ratio

Because of the presence of the sodium bond in the fuel pin, the gas plenum needs to be located above the metal fuel slug. The metallic fuel requires a sufficiently long upper gas plenum to maintain a low pressure on the cladding by providing sufficient volume to contain the bond sodium expelled from the fuel region and to accommodate released fission gas [Hofman 1997]. The length of the upper gas plenum is dependent on the burnup and cladding materials. Based on the irradiation experiences of the metallic fuels till 10-20at% with HT9 cladding, the plenum-to-fuel volume ratio is recommended to be 1.4 or higher. Plenum pressure impacts the transient performance the most. At elevated temperatures, the clad failure margin could come down very rapidly if the clad hoop stress is 100 MPa or more. It is a good practice to keep the clad hoop stress below 50 MPa during the normal operation to allow for reasonable clad failure margin during the transients.

2.4.2 Coolant and cladding temperatures

The coolant temperature and flow rate for the metallic fuel with HT9 cladding are designed to mitigate the fuel/clad chemical interaction (FCCI). In particular, a critical design requirement is to maintain the inner cladding temperature below the eutectic formation between the metallic fuel and cladding. The eutectic formation temperature varies depending on the fuel alloy, cladding materials, and fission products (burnup). The eutectic formation starts at 650°C for high Pu content metallic fuels and at 715°C for U-10Zr [Hofman 1997, Nakamura 2001]. At steady-state, the peak inner cladding temperature is typically limited to 650°C while accounting for 3σ levels of confidence using hot channel factors (HCF) to minimize risks of FCCI. The HCF methodology and recommended values are described in [Waltar 2012, Section 10.4].

Another mode of fuel clad chemical interaction limiting the performance is the lanthanide attack to the clad inner surface. Lanthanides are insoluble in fuel. At elevated temperatures, they can diffuse into cladding and form brittle clad inner structure. X447 subassembly (SA) operated in EBR-II led to two fuel pin failures due to extensive lanthanide attack [Pahl 1993]. This mode of FCCI is significantly slower than eutectic formation but can be very significant during normal operation if the clad inner surface temperature is above 600°C. Since lanthanides are produced with fission, at high burnup metal fuel can be more corrosive compared to low burnup fuel. Hence, the power/flow history could also make a serious impact on the performance.

During the transient at elevated temperatures the main clad failure mode is thermal creep rupture augmented by the clad wastage formation. Creep rupture is highly dependent on operating temperature, stress and the duration.

Considering the inner cladding temperature limit and acceptable flow rate and pressure drop, typical inlet/outlet coolant temperatures used in metallic-fueled SFRs are 360°C/510°C, which is ~40°C lower than traditional oxide fuel. Increased coolant temperature would be possible if the core is designed at a low power density or higher flow rate to meet the inner cladding temperature limit recommended for metallic fuel.

2.4.3 Irradiation performance

Use of ferritic–martensitic HT9 cladding with recommended smeared density and fuel-to-plenum ratios can ensure reaching 10at% burnup level and expected to have satisfactory behavior up to 20at% [Crawford 2007]. Experimental data confirmed HT9 cladding capability to withstand peak dose of 200 dpa or peak fast neutron (>0.1 MeV) fluence up to 4×10^{23} n/cm² (EBR-II conditions). Higher fast fluence may be available but haven't been demonstrated yet.

During normal operation, cladding at majority of the axial locations operates at irradiation creep dominant temperatures. Depending on the coolant conditions, the upper axial regions may operate in thermal creep dominant temperatures. Irradiation creep induced clad dilatation is expected at high burnups mainly due to solid fission product swelling induced fuel clad mechanical interaction and sintering of the fuel porosity. Irradiation creep has benign effect on the clad failure compared to thermal creep. Hence, it can easily be accommodated up to 2% clad hoop strain. On the other hand, when the clad thermal creep strain is above 1%, it could lead to significant decrease in clad failure margin.

2.4.4 Inherent Safety

In a scoping design stage, the inherent safety features of the core are confirmed using quasi-static reactivity balance equations [Wade 1989]. Then, the inherent safety features of the final core design are ensured by performing transient simulations with a reactor safety analysis code like SAS4A [Fanning 2017] under various transient scenarios (UTOP, ULOF, ULOHS, etc.). The high thermal conductivity and small stored Doppler reactivity from a low operating temperature of metallic fuel tend to favor inherent safety behavior under these postulated unprotected accidental scenarios [Chang 2007].

2.5 Recommendation for modelling thermal-physical properties of metallic fuel

A. Karahan, Argonne National Laboratory (ANL)

This section provides recommendations on the U-Pu-Zr metal fuel properties and identifies possible approaches to model the key physical phenomena that are essential to predict the steady state and transient behavior.

2.5.1 Thermo-physical properties

2.5.1.1 Fuel thermal conductivity

Unirradiated metal fuel thermal conductivity given in [Hofman 1985] can be adopted. Furthermore, [Hofman 1985] suggests models for porosity correction factor to the thermal conductivity. In addition, sodium infiltration into porosity at outer radial sections can possibly be modeled using the data in [Bauer 1995] and [Ohta 2015]. [Ohta 2015] includes sodium length above the top of the fuel for metallic fuel irradiated in PHENIX.

2.5.1.2 Enthalpy, specific heat and melting temperatures

Enthalpy, specific heat, heat of fusion, melting temperatures can be found in [Hofman 1985].

2.5.1.3 Phase transitions

Phase diagrams and transition temperatures can be found in [Hofman 1985]. In addition, simplified phase transition temperatures can be found in [Karahan 2009].

2.5.1.4 Density and thermal expansion

Fuel density and thermal expansion correlations can be found in [Hofman 1985].

2.5.2 Fuel swelling and fission gas release

Fuel swelling of metal fuels is significantly different compared to oxide fuels. Fission gas nucleates bubbles in both phase and grain boundaries. As a consequence of 3D swelling, a significant amount of free space between fuel and cladding or low fuel smear density is required to form the interconnected open porosity network. Formation of interconnected porosity network significantly reduces the fuel swelling, allows path for the fission gas release and accommodates solid fission product swelling at the expense of pore sintering. Fission gas release pressurizes the free volume of the pin. Perfect gas law can be applied assuming

mechanical equilibrium between fuel porosity volume and gas plenum volume. Solid fission product swelling can be modeled linearly with burnup with a rate of 1.5 % / at % burnup.

Sophisticated models are available to model the fuel swelling and fission gas release [Karahan 2009, Karahan 2013]. Alternatively, a simple empirical model can be adopted to model the steady state behavior although it has limitations. Eq. 2.2.1 at [Karahan 2009] suggests an exponential correlation for fission gas release as a function of burnup. Fuel swelling can also be modeled as a function of burnup. As given above, solid fission product swelling increases linearly with burnup. Swelling can be modeled as sum of solid fission product and fission gas induced bubble/porosity swelling. For the total fuel swelling, it can be assumed that the swelling linearly increases with burnup up to 2 at% and fuel is assumed to be totally swollen by this burnup. Subtracting the solid fission product swelling from the total swelling results in the fuel porosity. Upon hard contact between the fuel and cladding, porosity sintering takes place to accommodate the solid fission product swelling, driving the interfacial stress between fuel and cladding above the plenum pressure. Hydrostatic stress required to sinter fuel porosity can be modeled as a function of fuel creep and porosity as developed by various authors [Karahan 2009, Ogata 1999] or a more simplified model can be adopted.

2.5.3 Mechanical behavior and properties

Elastic constants can be found in [Hofman 1985]. Fuel creep relations as a function of temperature and stress can be found in [Gruber 1987]. Typically, the fuel is porous and pore sintering controls the stress at hard contact. Interconnected porosity also limits any residual stress buildup. During start up, fuel cracking limits axial expansion via earlier radial contact with the cladding. As a result, the fuel swelling is anisotropic, biased towards the radial direction. The fuel axial elongation can be between 1 to 9 % depending on operating conditions, fuel pin geometry and Pu content [Karahan 2009]. Typically, the fuel first reaches to soft contact condition where fuel clad mechanical interaction is still minor but fuel is axially restrained such that majority of the fuel swelling advances in radial direction. When the fuel comes to hard contact with the cladding where fuel swelling is complete, the contact stress sinters the open porosity accommodating for the solid fission product swelling. As the fuel porosity diminishes and plenum pressure increases at high burnup, interfacial stress may increase substantially and lead to clad failure.

During the transients, upon eutectic formation between fuel and cladding, softer and frictionless fuel tends to expand in axial direction with very low interfacial stress between fuel and cladding.

2.5.4 Fuel constituent redistribution

At power, metal fuel phases have different chemical affinity for U, Zr atoms leading to radial redistribution [Kim 2006, Hofman 1996]. Zr depleted and enriched radial regions may form. The difference in solidus temperature between these regions can be as high as 300 K. As fuel's Pu content increases, both phase transition temperatures decreases and diffusivities increases leading more extensive redistribution for high Pu content fuels. Fuel constituent redistribution may also affect the radial power distribution and local thermal conductivity.

To model this phenomenon, one needs to adopt a diffusion model based on thermo-transport theory [Karahan 2009, Kim 2006, Hofman 1996]. For simplified analysis, it can be ignored.

2.5.5 Clad wastage

During normal operations, Lanthanide atoms, which are insoluble in fuel, tend to diffuse to the cladding and form brittle structure at the clad inner surface [Pahl 1993]. If excessive, it could be life limiting process [Pahl 1993]. A simplified diffusion model such as described in [Karahan 2009] can be adopted to model the clad inner wastage.

During the transient, once slow eutectic temperature is exceeded, fuel surface liquefaction and clad dissolution takes place [Cohen 1993]. Slow eutectic forms below 1080 °C. The critical temperature data can be found in [Nakamura 2001]. Above this critical temperature rapid eutectic takes place which can dissolve the cladding on the order of a second.

The empirical correlation given for both slow and rapid eutectic in [Bauer 1987] can be adopted for simplified studies.

2.5.6 Clad properties and failure

HT9 clad properties can be found in [Karahan 2009]. Note that the thermal creep correlation for HT9 given in [Karahan 2009] was found to be on the conservative side. Improved correlations can be found at SAS4A/SASSYS-1 Version 5.7 [ANL, 2023].

To characterize the clad failures, Cumulative Damage Fraction (CDF) models, 1% thermal creep criterion and excessive wastage criterion can be adopted. Experiments indicated that clad failures are expected above 1% thermal creep strain. Typically, during steady state and transient, it is recommended to have clad wastage below 25% and 50% of the initial clad thickness in steady state and transients, respectively.

3 ESFR-M fuel and core design

A. Jiménez-Carrascosa and K. Mikityuk, Paul Scherrer Institut (PSI)

E. Fridman, Helmholtz Zentrum Dresden Rossendorf (HZDR)

Based on the feedback resulting from the review of both UK and US experience in metallic-fueled SFR systems, this section deals with the pre-design of the ESFR-M (European Sodium Fast Reactor with Metallic fuel). The ESFR-M is conceived as a modified version of the design developed in the frame of the ESFR-SMART project [Rineiski 2022], for which the selected fuel was (U-Pu)O₂ – a mixed uranium-plutonium oxide (MOX).

At this designing phase, the ESFR-M concept is assumed to preserve most of the features implemented in the reference ESFR-SMART core (ESFR-MOX). The aim is to evaluate the impact of the new metallic fuel type on core performance in comparison with the reference MOX core. Lastly, the ESFR-M core model will be subject to modifications according to the potential feedback provided by fuel performance and safety analyses to be carried out in subsequent tasks.

Due to the experience that the United States collected in U-Pu-Zr metallic fuel and taking into account the amount of available experimental feedback, a ternary U-Pu-Zr fuel alloy with 10 wt% zirconium has been selected as a reference for the ESFR-M design. Then, this section firstly presents a brief overview of main recommendations provided by ANL for designing this type of SFRs. Then, the designing approach is described along with main modifications implemented with respect to the reference ESFR-SMART core. Finally, a preliminary neutronic analysis is performed with the aim of selecting the most appropriate core configuration. It is important to note that a more detailed neutronic analysis will be carried out in next iterations.

3.1 Overview of main recommendations for metallic-fuel SFR design

Before addressing the design of the ESFR-M core, it is worth recalling the most important criteria provided in Section 2.4 to be taken into account in the procedure. As previously stated, selected parameters are considered to be licensable by the U.S. regulator via the available experimental data from different facilities.

Concerning the pin design specifications, a sodium-bonded fuel pin is preferred, with a smeared density of around 75% in order to keep room for fuel radial swelling as burnup increases. At some point, the fuel slug is expected to reach the inner surface of the cladding. Part of the bond sodium (15 to 30 %) is displaced above the fuel slug region to the upper gas expansion plenum while the remaining bond sodium infiltrates into fuel porosity. Neutronic analyses should account for the quick fuel swelling, both radially and axially, as a function of irradiation.

Differently from MOX-fueled cores, the gas plenum should be located above the metal fuel slug to provide sufficient volume for not only fission gas released from the fuel, but also the bond sodium expelled from the fuel region by the irradiation-induced swelling. As a result, the plenum-to-fuel volume ratio is recommended to be 1.4 at least, located just above the sodium bond-free level (1-2 cm above the fuel slug).

Past irradiation experiments reported a good performance of HT9 as cladding material, so that the ODS traditionally selected for the ESFR fuel pin should be replaced by the HT9 cladding. The pin outer cladding diameter is suggested to range from 0.584 to 0.94 cm, with a cladding thickness of 0.038-0.051 cm. The current design for the ESFR fuel pin consists of a cladding for which the outer diameter and cladding thickness are 1.0777 and 0.0526 cm, respectively.

Thus, the fuel pin dimensions are slightly out of range but a thicker fuel pin might be also acceptable as long as both the smeared density and the plenum-to-fuel volume ratios fulfill the required specifications.

Finally, it is worth mentioning that the metallic fuel vector, both the uranium and plutonium composition, corresponds to those applied in the ESFR-SMART project, but the fuel density information is retrieved from [Hofman 1985] for the alloy U-15Pu-10Zr. In that case, the “as-cast” alloy density is of 15.67 g/cm³, but most importantly, temperature-dependent density and thermal expansion are also provided.

3.2 ESFR-M fuel and core design

As aforementioned, the ESFR-M core design approach aims to maintain the MOX-fueled ESFR core specifications as much as possible relying on licensable designing parameters. This section firstly describes the proposed options for the ESFR-M configuration, highlighting the main differences compared to the reference ESFR design. According to selected options, the designing approach is then described along with detailed core specifications.

3.2.1 Proposed design options

The ESFR-M core design is expected to preserve the core performance achieved for the ESFR-MOX described in [Rineiski 2022]. That is, the reactor power is set to 3600 MWth, with a fuel residence time of 2170 EFPD (Equivalent Full Power Days) following a multi-batch reloading scheme with 6 different batches. The ESFR-M core also consists of inner fuel (IF) and outer fuel (OF) core regions, loaded with 216 and 288 fuel SAs, respectively.

Then, the majority of proposal for the ESFR-M core design rely on minor geometry modifications as described in Table 4. This description is accompanied by evaluated material component volumetric fractions to depict the evolution of the proposed geometries (see Table 5).

Table 4: Proposed designing approaches for the ESFR-M core with respect to the current ESFR-MOX design.

	M1	M2	M3	M4
Core map	Same	Same	Same	Different
SA pitch	Same	Same	Reduced	Reduced
Number of fuel pins	Same	Same	Same	Different
Clad dimensions	Same	Reduced	Reduced	Reduced
Fuel dimensions	Reduced	Reduced	Reduced	Reduced
Spacer	Wire	Grid	Wire	Wire

Table 5: Core material volumetric fractions.

	ESFR-MOX	ESFR-M1	ESFR-M2	ESFR-M3
Fuel inner hole	5.54%	0.00%	0.00%	0.00%
Fuel	44.28%	33.95%	33.95%	37.06%
Gap/sodium bond	2.50%	18.37%	11.31%	12.34%
Cladding	11.94%	11.94%	11.15%	12.17%
Sodium coolant	23.47%	23.47%	31.31%	25.62%
Wrapper	8.23%	8.23%	8.23%	8.58%
Inter-assembly sodium	4.06%	4.06%	4.06%	4.24%
Smeared density		64.90%	75.00%	75.00%

The first option, ESFR-M1, introduces a limited modification compared to the ESFR-MOX core, with a reduced fuel diameter and therefore increased fuel-clad gap, while the rest of specifications are preserved. The main assumption was that the total HM mass should be the same as in the ESFR-MOX core.

Similarly, the ESFR-M2 option considers a reduction of the fuel pin diameter and, therefore, of the cladding dimensions and aims at meeting the smeared density requirement of 75% (not met in M1, as it can be observed in Table 5). As a result, this option proposes an increased fuel lattice pitch-to-diameter ratio, leading to the need of introducing a grid spacer instead of the spacer wire traditionally selected for the ESFR-MOX design. This option is expected to perform slightly better than the ESFR-M1 in terms of initial reactivity excess due to the reduced amount of cladding. On the other hand, the sodium density related reactivity effect (including voiding reactivity effect) is expected to deteriorate becoming more positive because of the higher amount of sodium coolant outside the fuel pin. This issue is to be investigated during analysis of hypothetical accidental conditions of unprotected loss of flow, in particular by modeling the sodium boiling, if occurring. Additionally, the impact of the grid spacer on the thermal-hydraulic performance should be also evaluated.

The next iteration to ESFR-M2 is proposed as ESFR-M3, where the fuel pin dimensions are reduced but the SA is compacted, reducing sodium volume fraction with respect to M2 and coming back to the use of the wire spacers. The core size would be then reduced even though the core map and the reloading scheme remain as in the initial ESFR-MOX design. Figure 7 shows the radial layout of the reference ESFR-MOX SA, as well as the three options (M1-M3) proposed for the ESFR-M design.

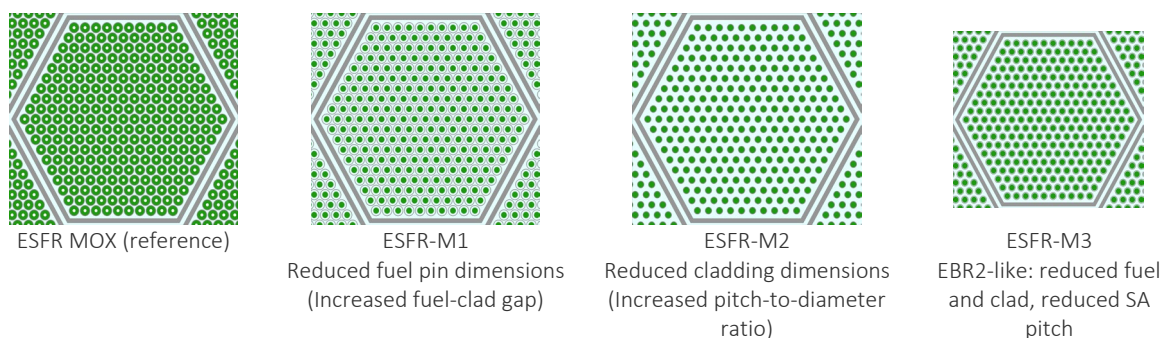


Figure 7: SA designs of reference ESFR-SMART as well as three options proposed for ESFR-M.

Concerning the axial description of the M-designs, a fission gas plenum should be located above the fuel slug. In this case the efficiency of the sodium plenum above the pin bundle in case of voiding is expected to be negligible, while the sodium voiding in the long upper gas plenum region results in a moderate negative reactivity. This is in contrast to the ESFR-MOX configuration, where the gas plenum is located below the fuel region and the sodium plenum – just above the fuel region. In any case, a preliminary characterization of the sodium void effect for selected options is provided in Section 3.3.

It is worth mentioning that the ESFR-M4 configuration relying on a completely new maps for batches and cooling groups, might be also considered but it introduces major modifications to the core map, which would require a complete re-design study. Nonetheless, this proposal is in line with past experimental facilities, such as the EBR-II [Briggs 1995], and smaller metallic-fueled core designs [Kim 2009]. At this point, this is not the goal of the current approach and, therefore, the ESFR-M4 option is discarded for the moment but to be recalled in future iterations.

Then, the designing approach for the initial version of the ESFR-M core will firstly rely on the ESFR-M1 option, while ESFR-M2 and M3 are not discarded and they might be considered to ensure the fulfillment of all recommended parameters.

3.2.2 ESFR-M designing approach

The ESFR-M design approach is mainly based on the assumption that the total heavy metal (HM) mass should be the same as in the ESFR-MOX core. Additionally, equal Pu content should be used in the inner and outer core zones, applying the same Pu and U vectors, provided in Table 6. Compared to the ESFR-MOX, the ESFR-M avoids the fuel pellet inner hole even though annular metallic fuel design might be promising in terms of fuel performance [Miao 2019]. Fertile regions are also removed from the core, but it is important to note that uranium mass corresponding to fertile blankets in the ESFR-MOX core is preserved when calculating the heavy metal inventory to be loaded in the ESFR-M design. The first step addresses the evaluation of the total fuel mass, and its components, loaded in the ESFR-MOX core.

Table 6: Uranium and plutonium vectors used for fresh fuel composition.

Vector	Isotope	Mass (%)
Uranium	U-235	0.25
	U-238	99.75
Plutonium	Pu-238	3.571
	Pu-239	47.38
	Pu-240	29.66
	Pu-241	8.231
	Pu-242	10.38
	Am-241	0.778

Table 7 shows the ESFR-MOX fuel mass at nominal conditions, with around 79 MT of HM, which is the value to be maintained throughout the ESFR-M1 designing approach. As mentioned earlier, the uranium mass also accounts for the fertile blankets, leading to an averaged Pu content of 15.31%. The definition of the ESFR-M1 fuel vector will initially rely on this Pu content, with further sensitivity studies in this regard.

As a result, the U-Pu-Zr fuel isotopic composition can be directly defined based on the main selected characteristics, which are summarized in Table 8. Subsequently, Table 9 provides the number densities for the metallic fuel composition, both at cold and operating conditions. It should be noted that, according to [Hofman 1985], the fuel density decreases by around 3% for the expected working temperature.

Once the fuel composition is defined, the required fuel volume can be calculated straightforwardly taking into account the constant HM mass. Thus, the fuel volume is required to be of 5.72 m³, while it is 8.76 m³ for the ESFR-MOX core. Accordingly, the fuel pellet diameter as well as its height can be defined to fulfill with the required fuel volume. At this point, two different alternatives arise:

- The fuel pellet diameter can be set so that the smeared density requirement (75%) is accordingly fulfilled, considering the cladding dimensions as they are in the ESFR-MOX core. In that case, the active core height would be significantly reduced as compared with the reference design, which will reinforce the leakage component and thus requiring the addition of a dedicated axial reflector.

- On the other hand, the axial dimensions can be fixed reasonably close to the ESFR-MOX core. The target parameter in this case becomes the fuel diameter. In this case, the inner fuel height is set to 75 cm while the outer fuel height should be kept to 95 cm, both at cold conditions. Following this approach, the axial description of the ESFR-M core is practically equivalent to the ESFR-MOX core except the location and the height of the gas plenum.

The second route is selected with the aim of keeping the core axial description as defined for the ESFR-MOX core [Rineiski 2018]. Then, giving the fuel axial dimensions for each core region, inner and outer, the fuel diameter should be set to 0.783 cm, leading to a smeared density of around 65% when the cladding radius is kept as in the ESFR-MOX. This smeared density is indeed lower than the recommended value, so that further analyses will be required for assessing a modification of cladding dimensions to reach a smeared density of 75%.

In summary, the ESFR-M1 proposal is selected as first iteration, with a reduced fuel diameter as compared with the ESFR-MOX configuration, but keeping fixed the rest of dimensions as they are currently set.

Table 6: Uranium and plutonium vectors used for fresh fuel composition.

Vector	Isotope	Mass (%)
Uranium	U-235	0.25
	U-238	99.75
Plutonium	Pu-238	3.571
	Pu-239	47.38
	Pu-240	29.66
	Pu-241	8.231
	Pu-242	10.38
	Am-241	0.778

Table 7: ESFR-MOX fuel mass at nominal conditions.

ESFR-MOX fuel component	Mass (MT)
Uranium	66.8408
Plutonium*	12.0847
HM	78.9255
Total fuel	89.4299

* americium is included in the plutonium vector

Table 8: U-Pu-Zr- fuel characteristics.

Inner fuel Pu content (%wt)	15.31
Outer fuel Pu content (%wt)	15.31
Zirconium content (%wt)	10.00
Fuel average density at cold conditions (g/cm ³)	15.80
Theoretical fuel density (%)	100
Average fuel temperature at nominal conditions (K)	900

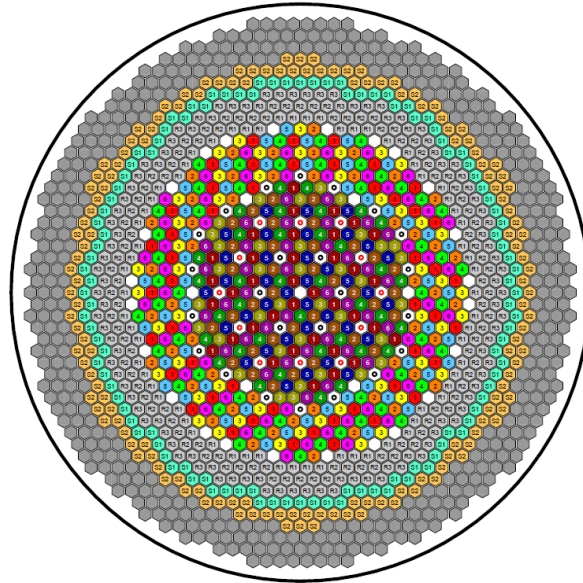
Table 9: Isotopic composition of U-Pu-Zr metallic fresh fuel (at cold and nominal operating conditions).

		298 K	900 K
Nuclide	ID	ND, 1/b-cm	ND, 1/b-cm
Zr-90	4090	5.44516E-03	5.28319E-03
Zr-91	4091	1.17438E-03	1.13945E-03
Zr-92	4092	1.77555E-03	1.72273E-03
Zr-94	4094	1.76101E-03	1.70863E-03
Zr-96	4096	2.77786E-04	2.69522E-04
U-235	92235	7.71376E-05	7.48430E-05
U-238	92238	3.03891E-02	2.94852E-02
Pu-238	94238	1.96693E-04	1.90842E-04
Pu-239	94239	2.59904E-03	2.52172E-03
Pu-240	94240	1.61999E-03	1.57180E-03
Pu-241	94241	4.47711E-04	4.34393E-04
Pu-242	94242	5.62048E-04	5.45329E-04
Am-241	95241	4.23723E-05	4.11119E-05
Total	Total	4.63680E-02	4.49887E-02

3.2.3 ESFR-M core design specifications

The ESFR-M core layout corresponds to the configuration defined in the ESFR-SMART project [Rineiski 2018]. Figure 8 shows the ESFR radial core layout featuring a 6-batch reloading pattern. The core is controlled by 24 control and shutdown devices (CSD) and 12 dedicated shutdown devices (DSD). Additionally, 31 corium discharge tubes (CDT) were introduced into several locations, including the central position, the boundary between IF and OF regions, and the active core periphery, which is surrounded by 3 reflector rings. Extended analysis should provide insight into the possibility of removing CDT for the ESFR-M design due to the intrinsic core features.

Concerning the axial core map, major changes affect the fuel SAs while the rest only require minor adjustments to keep the consistency with the fissile fuel location. Accordingly, Figure 9 depicts the changes introduced in the ESFR-M core design with respect to the ESFR-MOX core, including a radial cut of the fissile region for each configuration. It can be clearly seen that the active part is now located in a lower position with the aim of providing space for the addition of the upper gas plenum. For the ESFR-M configuration, the fuel pin consists, from bottom to top, of the lower plug, the steel blanket, the fuel slug, free level of the bond sodium, the gas plenum, and the upper plug.





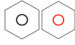



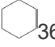
	IF SA	6 batches × 36
	OF SA	6 batches × 48
	CSD / DSD	24 / 12
	Reflector	66 / 96 / 102
	Spent IF storage	3 batches × 36
	Spent OF storage	3 batches × 48
	CDT	31

Figure 8: ESFR radial core layout.

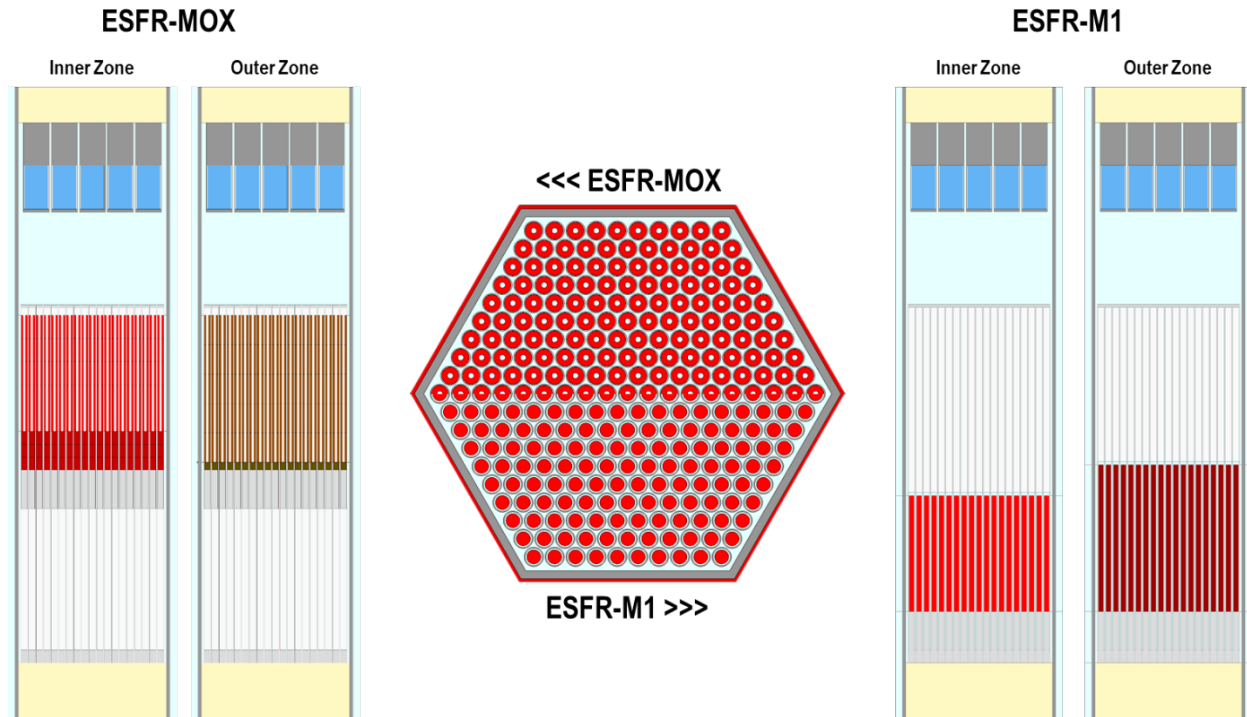


Figure 9: Axial layout of the ESFR-MOX and ESFR-M1 fuel sub-assemblies with a radial cut corresponding to the fissile region of each configuration.

This design fulfills the requirement related to the fuel-to-plenum volume ratio of 1.4 or higher, being of around 1.6 for the inner fuel pin. Above the fuel pin lattice, the sodium plenum and the top absorber are kept as they are in the ESFR-MOX design, but it is important to note that the sodium plenum efficiency will be strongly reduced. Further modifications will depend on the core behavior during transient sequences and the impact of the increased (with respect to ESFR-MOX) positive sodium density related reactivity effect in the fissile region (including sodium voiding) as well as the reduced Doppler effect. Nonetheless, a more detailed analysis of the SA axial design options, including removal of the sodium plenum, will be performed in next designing phases. Additionally, the consideration of the sodium voiding and related positive reactivity effect in the metallic core should be analyzed within the framework of safety analysis.

The axial dimensions are provided for the ESFR-M inner and outer fuel sub-assemblies in Table 10, where expansions from cold to nominal conditions are assumed to be as for the ESFR-MOX core. This assumption needs to be revisited in next iterations since the nominal temperatures are expected to be lower for the ESFR-M compared to the ESFR-MOX core. This also applies to the metallic fuel, for which more consistent thermal expansions should be considered.

Following the changes introduced for the fuel SAs, the axial dimensions of control rods, corium discharge tube and radial reflector assemblies are accordingly updated as shown in Table 11, Table 12 and Table 13, respectively. It is important to note that, at this stage, the bottom of the control rods is aligned with the top of the bond sodium free level (i.e., 2 cm above the outer fuel region) at parking position. Once the fuel swelling is considered, the parking position will be located at the expanded upper fuel position. Additionally, the height of the SA slightly increases when moving from the ESFR-MOX to the ESFR-M design, so that all the SAs are updated similarly.

It should be noted that the head and foot regions are modelled as homogeneous mixtures inside the SA wrapper. The sodium plenum region is modelled assuming sodium inside the SA wrapper. The bond sodium above the fuel slug appears as a new axial layer in the ESFR-M design. Thus it is modelled as sodium inside the fuel pins, with the same density and temperature as the sodium located in the fuel-cladding gap.

Even though the radial geometry remains practically unmodified as compared with the reference design, Table 10 provides detailed specifications for the ESFR-M1 fissile fuel SA with updated dimensions for the fuel slug. It is important to highlight that the same assumptions described in [Rineiski 2018] concerning the thermal expansions in the neutronics analysis for the ESFR-MOX core are also applied in this case. Moreover, it can be observed that ODS is kept as cladding material at this stage, but it should be replaced by HT9 cladding following the recommendations provided in Section 2.4.1. These minor adjustments will be implemented and evaluated in next Tasks, with the support of dedicated computational tools.

The radial description associated to the rest of SAs can be indeed retrieved from [Rineiski 2018] as well as the isotopic composition of structural materials, so that the full core model can be built straightforwardly.

Table 10: ESFR-M axial dimensions: inner and outer fuel.

#	Axial region	IF				OF			
		Region height (cm)		Cumulative height (cm)		Region height (cm)		Cumulative height (cm)	
		cold	nominal	cold	nominal	cold	nominal	cold	nominal
1	Foot	37.000	37.201	0.000	0.000	37.000	37.201	0.000	0.000
2	Lower plug	8.200	8.245	37.000	37.201	8.200	8.245	37.000	37.201
3	Lower steel blanket	25.000	25.136	45.200	45.446	25.000	25.136	45.200	45.446
4	Fissile	75.000	75.407	70.200	70.582	95.000	95.516	70.200	70.582
5	Sodium bond	2.000	2.011	145.200	145.989	2.000	2.011	165.200	166.098
6	Upper gas plenum	120.000	120.652	147.200	148.000	100.000	100.543	167.200	168.109
7	Upper plug	1.800	1.810	267.200	268.652	1.800	1.810	267.200	268.652
8	Sodium plenum	60.000	60.326	269.000	270.462	60.000	60.326	269.000	270.462
9	Reflector	1.800	1.810	329.000	330.788	1.800	1.810	329.000	330.788
10	Absorber	28.200	28.353	330.800	332.598	28.200	28.353	330.800	332.598
11	Reflector	27.600	27.750	359.000	360.951	27.600	27.750	359.000	360.951
12	Head	23.000	23.125	386.600	388.701	23.000	23.125	386.600	388.701
	sum	409.600	411.826	409.600	411.826	409.600	411.826	409.600	411.826

Table 11: ESFR-M axial dimensions: CSD and DSD.

#	Axial region	CSD				DSD			
		Region height (cm)		Cumulative height (cm)		Region height (cm)		Cumulative height (cm)	
		cold	nominal	cold	nominal	cold	nominal	cold	nominal
1	Foot	37.000	37.201	0.000	0.000	37.000	37.201	0.000	0.000
2	Na plenum	130.200	130.908	37.000	37.201	130.200	130.908	37.000	37.201
3	B4C nat.	45.000	45.244	167.200	168.109	45.000	45.244	167.200	168.109
4	B4C enrch.	40.000	40.217	212.000	213.353	50.000	50.272	212.200	213.353
5	Head	157.400	158.256	252.200	253.57	147.400	148.201	262.200	263.625
	sum	409.600	411.826	409.600	411.826	409.600	411.826	409.600	411.826

Table 12: ESFR-M axial dimensions: corium discharge tube.

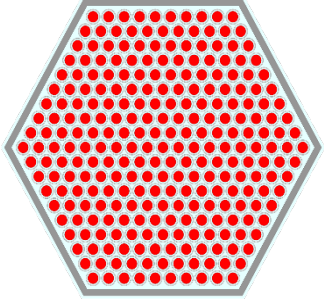
Core discharge tube		Region height (cm)		Cumulative height (cm)	
#	Axial region	cold	nominal	cold	nominal
1	Foot	37.000	37.201	0.000	0.000
2	Na plenum	292.000	293.587	37.000	37.201
3	Reflector	1.800	1.810	329.000	330.788
4	Absorber	28.200	28.353	330.800	332.598
5	Reflector	27.600	27.750	359.000	360.951
6	Head	23.000	23.125	386.600	388.701
	sum	409.600	411.826	409.600	411.826

Table 13: ESFR-M axial dimensions: radial reflector

Radial reflector		Region height (cm)		Cumulative height (cm)	
#	Axial region	cold	nominal	cold	nominal
1	Foot	37.000	37.201	0.000	0.000
2	Reflector	349.600	351.500	37.000	37.201
3	Head	23.000	23.125	386.600	388.701
	sum	409.600	411.826	409.600	411.826

Table 14: ESFR-M1 fissile fuel radial layout.

Fuel fissile			
Number of pins	271	Rad. expn. coeff.	Nominal dim.
pin pitch (cm)	1.1670		
		Nominal T, °C	ACE file T, K
Pellet material	U-Pu-Zr	627	900
Gap material	Na	470	900
Cladding material	ODS	470	900
	Cold dim.	Rad. expn. coeff.	Nominal dim.
Pellet radius (cm)			0.39168
Clad inner radius (cm)	0.4835	1.0056	0.48623
Clad outer radius (cm)	0.5358	1.0056	0.53886



3.3 Preliminary full core neutronics performance

The preliminary evaluation of the ESFR-M design performance includes the neutronics characterization of the new core at beginning of life (BOL) and the once-through burnup analysis using the calculational scheme used by [Fridman 2022a, Fridman 2022b] for the ESFR-MOX core. The main goal of this section is to estimate a neutronics behavior of the metallic-fueled core, with particular emphasis on a sensitivity to the plutonium content in the fuel. Thus, this study serves as basis for subsequent tasks of the ESFR-SIMPLE project, providing the initial ESFR-M core model to be in-depth evaluated in the following tasks.

In this work, calculations are carried out using Monte Carlo code Serpent 2.2 [Leppanen 2015] and based on the continuous-energy JEFF-3.1 nuclear data library [Koning 2007] to keep the consistency with the analysis carried out for the ESFR-MOX core. Concerning the burnup

calculations presented in this study, Serpent includes a built-in decay and depletion solver for which the radioactive decay data and neutron-induced fission product yields are also retrieved from JEFF-3.1 nuclear data library. For all calculations, the standard deviation of computed multiplication factor is ensured to be below 6 pcm.

It is important to mention that the irradiation-induced swelling is not modeled for neutronics analyses presented in this study. Thus, the metallic fuel dimensions and density remain constant along the irradiation time but extended neutronics simulations are required to implement the burnup-dependent fuel expansion as described in Section 2.4.1.2. A noticeable effect can be expected after accounting for the burnup-dependent swelling, with a decrease of the core reactivity, as described in [Hartanto 2016]. Then, as next step, a more realistic approach should be developed for the characterization of the core behavior in equilibrium cycle.

The modelling assumptions applying to the initial ESFR-M core burnup calculations are in line with those applied to the ESFR-MOX core [Fridman 2022b]. Thus, calculations are performed for a total of 2100 EFPD, without reloading and reshuffling. Along the burnup, all control devices are withdrawn to their parking position. Concerning the axial discretization of the fissile fuel, both the inner and the outer regions are subdivided into 5 burnable regions to account for different neutron flux exposures. Radially, the batch-wise discretization with 6 burnable regions in IF and OF is applied, assuming that all fuel sub-assemblies belonging to a certain batch form a single burnable region. This approach leads to a total of 60 burnable regions where the fuel composition is independently tracked.

Considering the described modelling assumptions, the burnup dependent core reactivity for the ESFR-M1 configuration is presented in Figure 10. As it can be seen, results for several core configurations with different Pu contents are also involved in this analysis but, in all cases, the total HM mass is kept the same. Additionally, this comparison also includes the core reactivity evolution for the ESFR-MOX core calculated by [Fridman 2022b].

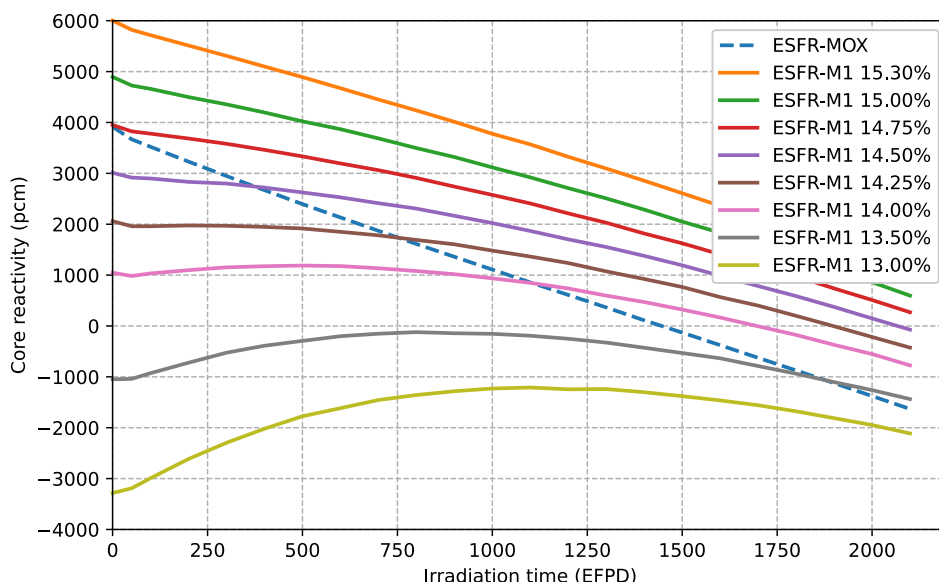


Figure 10: ESFR-M1 core reactivity as a function of irradiation time and Pu content.

Firstly, it should be noted that the reference ESFR-M1 design leads to a significantly higher reactivity value compared to the ESFR-MOX, being plutonium, uranium, and total HM masses equivalent in both designs. At BOL, the metallic-fueled design yields a higher core reactivity,

exhibiting an increase of around 2100 pcm. The reactivity swing is also reduced in the ESFR-M1 core, leading to a difference of 2700 pcm at End of Life (EOL).

Consequently, and more importantly, there is room for reduction of fissile fuel content in the ESFR-M1 core. Thus, while the total HM mass is kept constant, the Pu content is reduced so that the U mass increases accordingly. Figure 10 provides a sensitivity analysis regarding the impact of the Pu content on the burnup dependent core reactivity. It can be clearly seen a flattening of the core reactivity curve as the Pu content decreases, explained by increase of the breeding ratio.

Then, the Pu content can be reduced ensuring criticality at End of Cycle (EOC) and still providing a reactivity margin due to involved uncertainties, such as nuclear data. Even though the final Pu content should be fixed after performing a realistic transition to the equilibrium cycle and evaluating the EOC state, the configuration containing a Pu content of 14.00% appears to be promising at this point. Hence, Figure 11 provides a comparison concerning the evolution of U and Pu vectors for the ESFR-MOX and ESFR-M1 designs, including the latter two different fissile fuel vectors.

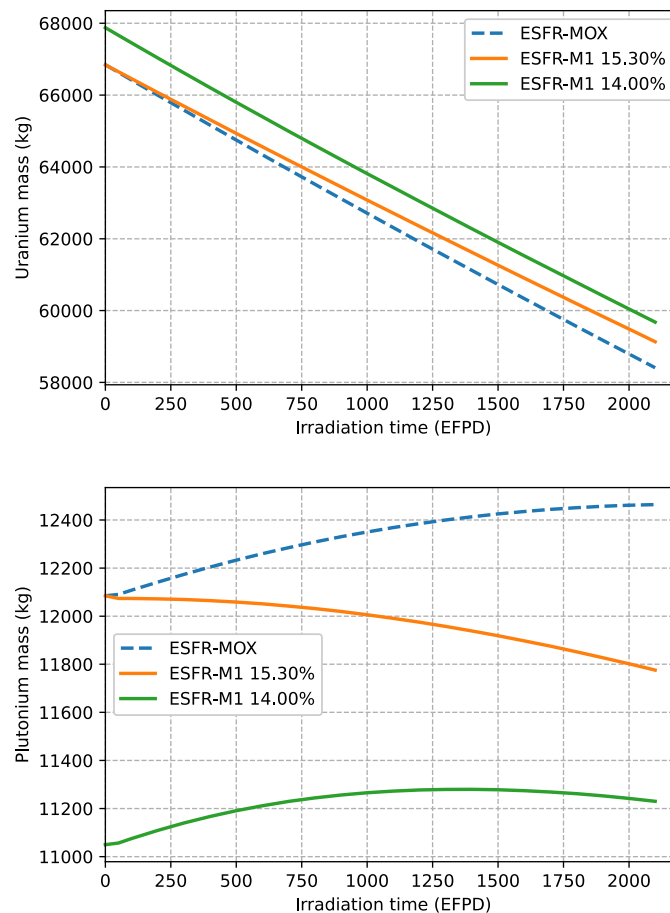


Figure 11: U (top) and Pu (bottom) vector masses evolution as a function of burnup for the ESFR-MOX and ESFR-M1 cores.

During the irradiation campaign, the uranium mass strongly decreased, mostly driven by the U-238 consumption for breeding Pu-239 (see Figure 12). It can be seen that the Pu-239 production rate is practically similar in the ESFR-MOX design and the ESFR-M1 core with 14.00% Pu content. On the other hand, the reference ESFR-M1 configuration operates with a

lower U-238 consumption rate and, consequently, produces a lower amount of Pu-239 in relative terms compared with the other configurations.

Then, as a result of this preliminary neutronics study, it can be concluded that the ESFR-M1 configuration with reduced Pu content shows an appropriate performance as compared to the reference ESFR-MOX core. As previously mentioned, this should be verified when a realistic burnup-dependent swelling model is implemented and extended to the evaluation of the equilibrium core performance.

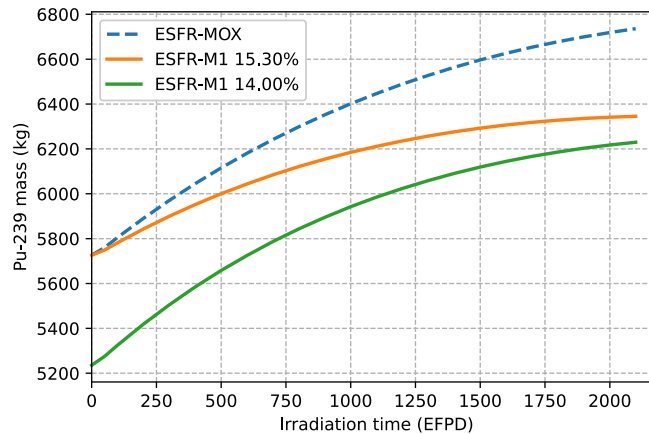


Figure 12: Pu-239 mass evolution as function of burnup for the ESFR-MOX and ESFR-M1 cores.

As part of this study, it is worth including in the comparison a further modified the ESFR-M2 version of the design (see Section 3.2.1). This modification considers the reduction of the cladding diameter with the aim of adjusting the design to the smeared density requirement. The ESFR-M1 designing approach led to a fuel pellet diameter for which the smeared density is around 65%, considering that the cladding diameter is kept as in the ESFR-MOX core. It can be argued that a higher smeared density is required to ensure the proper behavior of the system based on past operational experience. Thus, the transition of the ESFR-M1 to the M2 version is based on a reduction of the cladding diameter up to a smeared density of 75%.

Subsequently, the clad outer radius specified in Table 14 should be reduced up to 0.505 cm, keeping the thickness unchanged. This minor adjustment leads to a reduced fuel-cladding gap but the sodium mass inside the SA increases.

A slight improvement of the neutronics performance in point of the reactivity of fresh-fuelled core (by about 250 pcm) can be obtained in this case compared to the ESFR-M1 design, as shown in Figure 13. This reactivity excess can be mostly attributed to the lower mass of ODS loaded in the core, which is reduced by around 7%.

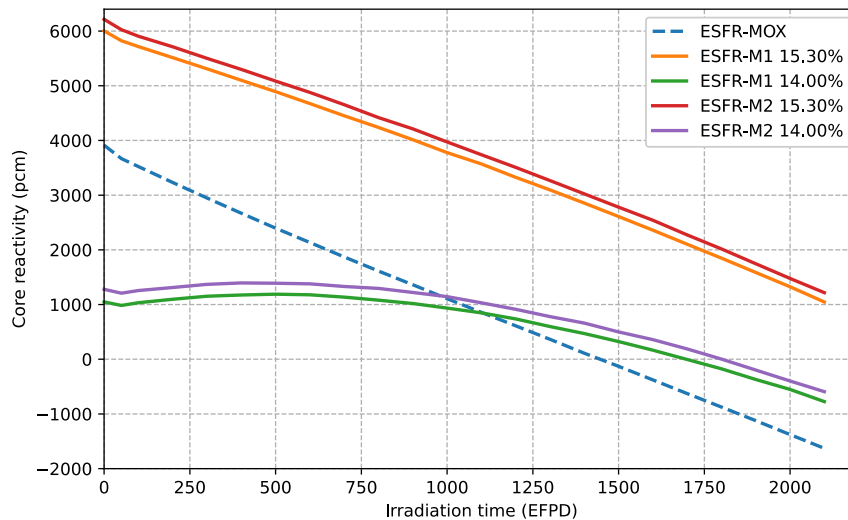


Figure 13: Core reactivity evolution as a function of burnup for both ESFR-M configurations.

Nevertheless, the higher amount of sodium coolant within the fuel SA will lead to a further degradation of the sodium void reactivity effect. This effect has been analyzed at BOL state and based on the voiding scenarios considered for the MOX-fueled core in the frame of the ESFR-SMART core [Fridman 2022a]. Thus, 5 sodium void scenarios are characterized as the difference in reactivity between the nominal and the voided states. These five voiding scenarios aim to characterize the sodium voiding at different core regions as follows:

- Void 1: voiding of inner fissile region,
- Void 2: voiding of outer fissile region,
- Void 3: voiding of everything above inner fissile region (including the sodium coolant surrounding the gas plenum pin lattice in the metallic-fueled core),
- Void 4: voiding of everything above outer fissile region,
- Void 5: the combination of all previous voiding scenarios.

In all cases, the sodium bond is not perturbed and the voiding only affects sodium outside the cladding. Sodium void reactivity values are compared in Figure 14 for the ESFR-MOX core and different considered ESFR-M configurations. On one hand, a significant systematic degradation of the reactivity effect can be already observed when comparing the ESFR-M1 design, with different Pu contents, and the ESFR-MOX core. This observation is a common trend when comparing the coolant voiding in the core active regions for metallic and oxide fuels, mostly driven by a stronger hardening effect of the neutron spectrum for the metallic fuel [Zhang 2016]. On the other hand, a reduced efficiency of sodium voiding of the above core region can be easily observed based on the results obtained for the void scenarios 3 and 4, being much lower than in the ESFR-MOX core. For these scenarios the effect is essentially driven by the voiding of the pin bundle at level of the upper gas expansion plenums and the sodium plenum plays an almost negligible role. Thus, next iterations should address the removal of the sodium plenum. Overall, the combination of the increased sodium void effect in the active part of the core and the lower efficiency of the above core region leads to a strong positive sodium void reactivity effect in all ESFR-M configurations. This must be considered in the following safety analyses, while it is important to mention that sodium boiling should not be expected in ESFR-M design so that the role of sodium voiding as a safety-related issue will be different as compared with ESFR-MOX core.

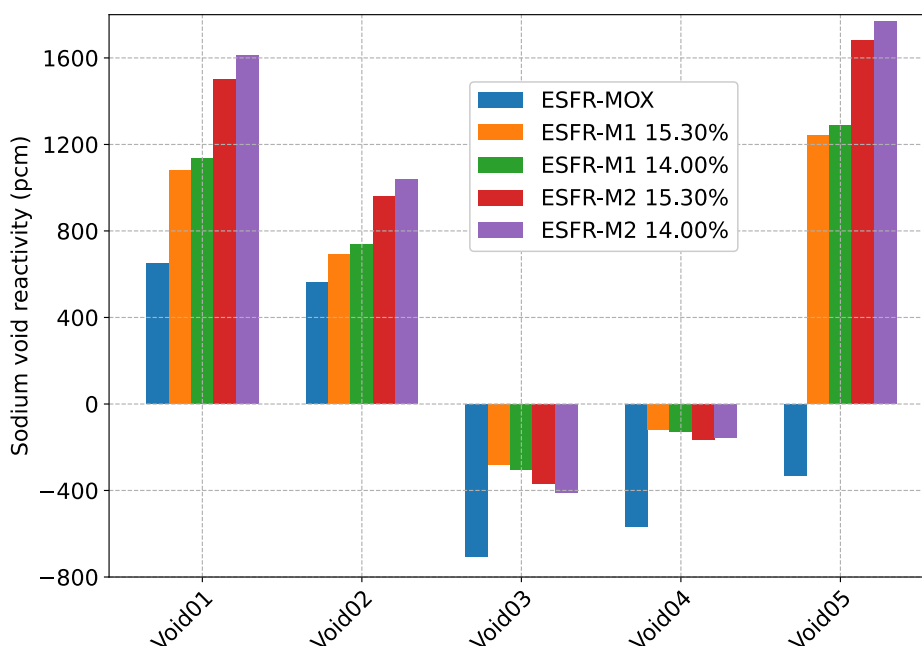


Figure 14: Sodium void reactivity for different ESFR configurations.

Additionally, the ESFR-M2 configuration exhibits a reinforced sodium void reactivity effect as compared to ESFR-M1 option, which is indeed due to the larger amount of sodium surrounding the fuel pin bundle in ESFR-M2. In both cases, a reduction of the Pu content points out an additional degradation of this safety coefficient. Nonetheless, if subsequent safety analyses involving consideration of all reactivity effects demonstrate that the ESFR-M2 configuration should be optimized in terms of safety and economic performance, another iteration can be proposed. This iteration can rely on the ESFR-M3 proposal, where all dimensions concerning fuel pin will remain as they are in ESFR-M2 but the SA pitch is reduced, leading to a more compact core design. In this case, the sodium mass surrounding the fuel pin lattice will be the close to the ESFR-M1 option, so that the sodium void effect should be reduced with respect to ESFR-M2. A preliminary evaluation of the sodium void reactivity effect shows similar values for both ESFR-M1 and M3 configurations, showing the latter slightly higher values in the active core region. Finally, it is worth mentioning that the ESFR-M3 option also provides room for investigating lower fissile fuel contents as compared with ESFR-M1 and M2 configurations.

4 Conclusions

This work addresses the first step concerning the study of an ESFR design with metallic fuel, describing the approach for designing a new core based on main recommendations provided by ANL. Additionally, this document serves as basis for further safety analyses so that these recommendations should be revisited throughout the whole safety analysis. It is important to mention that neutronics calculations carried out in this study rely on thermal expansions corresponding to the ESFR-MOX core, so that further updates will be required in this regard taking into account the ESFR-M operating conditions. In addition, differences between the ESFR-MOX and ESFR-M in terms of reactivity swing and reactivity excess should be in-depth analyzed.

As a result of this work, the ESFR-M1 with 14% Pu content can be envisaged as the reference design to be evaluated in Subtasks 1.2.4-1.2.6. This configuration shows an adequate performance in terms of core reactivity evolution as a function of irradiation time as well as a comparable mass balance between BOL and EOL states to the ESFR-MOX core.

As next step, the following neutronics simulations should be carried out in the frame of Subtask 1.2.4 to conclude on the adequacy of that configuration:

- A burnup-dependent swelling of the metallic fuel methodology should be developed in order to quantify the impact of this behavior in an accurate way. It may be expected a noticeable impact on the core reactivity swing due to this phenomenon with respect to the reference case, so that an increased Pu content might be expected.
- The simulation of the transition from BOL to the equilibrium cycle, and consequently to the EOC state, will provide information about the most limiting core state. Thus, further adjustments in the design might be needed as a function of core performance and safety parameters at EOC.

Additionally, it is worth mentioning that major modifications should be expected concerning the core design in accord with the metallic-fueled core intrinsic safety behavior. That is, the SA designs with sodium plenum above the pin bundle are not of interest for the metallic-fueled core, as sodium boiling is not considered to occur under transient sequences. Furthermore, the advantages of the application of the corium discharge tubes should be also reconsidered so that the core design will be iteratively updated in the frame of Task 1.2.

5 Bibliography

- [ANL 2023] Argonne National Laboratory, SAS4A/SASSYS-1, Version 5.7, Tech. Rep. ANL/NSE-SAS/5.7 (2023).
- [Bauer 1987] T. H. Bauer, et al., "Cladding Failure Margins for Metallic Fuel in the Integral Fast Reactor," CONF870812--22, Argonne National Laboratory, (1987).
- [Bauer 1990] T. H. Bauer, A. E. Wright, W. R. Robinson, J. W. Holland, E. A. Rhodes, "Behavior of Modern Metallic Fuel in TREAT Transient Overpower Tests," Nuclear Technology 92 (1990)
- [Bauer 1995] R. H. Bauer, H. W. Holland, "In-Pile Measurement of the Thermal Conductivity of Irradiated Metallic Fuel," Nuclear Technology, Vol. 110, pp. 407-421 (1995).
- [Beck 1968] W. N. Beck, R. J. Fousek, J. H. Kittel, "The Irradiation Behavior of High-Burnup Uranium-Plutonium Alloy Prototype Fuel Elements," ANL-7399, Argonne National Laboratory (1968).
- [Beck 1969] W. N. Beck, R. J. Fousek, "Fission Gas Release and Thermal Conductivity Measurement on U-5%Fs Irradiation in CP-5," Transaction of American Nuclear Society (1969).
- [Bette 1990] G. Bette and G. L. Hofman, "Run-Beyond-Cladding-Breach (RBCB) Test Results for the Integral Fast Reactor (IFR) Metallic Fuels Program," International Fast Reactor Safety Meeting IV, Snowbird, Utah (1990).
- [Betten 1983] P. R. Betten, J. H. Bottcher, B. R. Seidel, "Eutectic-Penetration-Induced Cladding Rupture in EBR-II Driver Fuel Elements," 1983 ANL Winter Meeting, CONF-831047-120 (1983).
- [Blake 1961] L. R. Blake, "Achieving High Burnup in Fast Reactors," Reactor Science and Technology 14 (1961).
- [Braase 2010] L. Braase, et al., "Advanced Fuels Campaign FY2010 Accomplishments Report," FCRD-FUEL-2011-000015, Idaho National Laboratory (2010).
- [Briggs 1995] L.L. Briggs, et al., "Safety Analysis and Technical Basis for Establishing an Interim Burnup Limit for Mark-V and Mark VA Fueled Subassemblies in EBR-II," ANL-NSE-1, Argonne National Laboratory, 2018.
- [Chang 1989] Y. I. Chang, "Integral Fast Reactor," Nuclear Technology 88 (1989).
- [Chang 2007] Y. I. Chang, "Technical Rationale for Metal Fuel in Fast Reactors," Nuclear Engineering and Technology, Vol. 39, 3 (2007).
- [Cohen 1993] A. B. Cohen, et al., "Fuel/cladding Compatibility in U-19Pu-10Zr/HT9-clad fuel at elevated temperatures," Journal of Nuclear Materials, Vol. 204, pp. 244-251, (1993).
- [Crawford 2007] D. C. Crawford, D. L. Porter, S. L. Hayes, "Fuels for Sodium-cooled Fast Reactors: US Perspective," Journal of Nuclear Materials 371 (2007) 202–231.
- [Crittenden 2019] G. Crittenden, C. Brown, "UK Liquid Metal Fast Breeder Reactor Core Fuels and Materials," NNL-14884 (Issue 1), National Nuclear Laboratory (2019).
- [Einziger 1979] R. E. Einziger, "Performance of EBR-II Mark-II Metallic Driver Fuel up to 675 °C," ANS International Conference on Fast Breeder Reactor Fuel Performance, CA (1979).
- [Einziger 1980] R. E. Einziger, B.R. Seidel, Nuclear Technology 50 (1980).
- [Fanning 2017] T.H. Fanning, A. J. Brunett, and T. Sumner, eds., The SAS4A/SASSYS-1 Safety Analysis Code System, Version 5, ANL/NE-16/19, Nuclear Engineering Division, Argonne National Laboratory, March 31, 2017.
- [Fiorini 2011] G. L. Fiorini and A. Vasile, "European Commission – 7th Framework Programme: The Collaborative Project on European Sodium Fast Reactor (CP ESFR)," Nuclear Engineering and Design, 241, 3461-3469 (2011).
- [Fistedis 1987] S. H. Fistedis, et al., "The Experimental Breeder Reactor II Inherent Safety

- Demonstration,” North-Holland (1987).
- [Fridman 2022a] E. Fridman, et al., “Neutronic Analysis of the European Sodium Fast Reactor: Part I – Fresh core results,” J. Nuclear Engineering and Radiation Science, Vol. 8(1), 011301 (2022).
- [Fridman 2022b] E. Fridman, et al., “Neutronic Analysis of the European Sodium Fast Reactor: Part II – Burnup results,” J. Nuclear Engineering and Radiation Science, Vol. 8(1), 011302 (2022).
- [Gruber 1987] E. E. Gruber, et al., “Gas Bubble Growth Mechanisms in the Analysis of Metal Fuel Swelling,” Proc. 13th Int. Symp. (Part-I) Radiation Induced Changes in Microstructure, ASTM-STP-955, p. 432, (1987).
- [Hartanto 2016] D. Hartanto, et al., “Impacts of burnup-dependent swelling of metallic fuel on the performance of a compact breed-and-burn fast reactor,” Nuclear Engineering and Technology, 48(2), 330-338 (2016).
- [Hilton 2006] B. A. Hilton, D. L. Porter, S. L. Hayes, 2006 ANS Annual Meeting, American Nuclear Society, La Grange Park, IL, Reno, NV (2006).
- [Hofman 1985] G. L. Hofman, et al., “Metallic Fuels Handbook,” ANL-IFR-29, Argonne National Laboratory, (1985).
- [Hofman 1990] G. L. Hofman, R. G. Pahl, C. E. Lahm, D. L. Porter, “Swelling Behavior of U-Pu-Zr Fuel,” Metallurgical Transactions A, Vol. 21 (1990).
- [Hofman 1994] G. L. Hofman, L. C. Walters, “Nuclear Technology”, VCH Verlagsgesellschaft mbH (1994)
- [Hofman 1996] G. J. Hofman, S. L. Hayes, M. C. Petri, “Temperature Gradient Driven Constituent Redistribution in U-Zr Alloys,” J. of Nuclear Materials 227 (1996).
- [Hofman 1997] G. J. Hofman, L. C. Walters, and T. H. Bauer, “Metallic Fast Reactor Fuels,” Progress in Nuclear Energy, Vol. 31 (1997), 83-110.
- [Karahan 2009] A. Karahan, “Modelling of thermo-mechanical and irradiation behavior of metallic and oxide fuels for sodium fast reactors,” Ph. D. Thesis Dissertation, Massachusetts Institute of Technology, (2009).
- [Karahan 2013] A. Karahan, et al., “Extended fuel swelling models and ultra high burn-up fuel behavior of U–Pu–Zr metallic fuel using FEAST-METAL,” Nuclear Engineering and Design, Vol. 258, pp. 26-34, (2013).
- [Kim 2006] Y. S. Kim, S. L. Hayes, G. L. Hofman, A. M. Yacout, “Modeling of Constituent Redistribution in U-Pu-Zr Metallic Fuel,” J. of Nuclear Materials 359 (2006).
- [Kim 2009] T. K. Kim, et al., “Core design studies for a 1000 MWth Advanced Burner Reactor,” Annals of Nuclear Energy 26, 331-336 (2009).
- [Kim 2010] T. K. Kim and C. Grandy, “Assessment of Fission Gas Vented Fuel Impact with Advanced Burner Reactor,” PHYSOR 2010 – Advances in Reactor Physics to Power the Nuclear Renaissance, Pittsburgh (2010).
- [Kittel, 1971] J. H. Kittel, J. A. Horak, W. N. Beck, R. J. Fousek, “Irradiation Behavior of Uranium-Fissium Alloys,” ANL-6795, Argonne National Laboratory (1971).
- [Koning 2007] A. J. Koning, et al., “The JEFF evaluated nuclear data project,” Proc. of International Conference on Nuclear Data for Science and Technology, 721-726 (2007).
- [Konings 2012] R. J. Konings, “Comprehensive Nuclear Materials,” Elsevier Ltd (2012).
- [Kryger 1969] B. Kryger, “Contribution to the Study of the Fission-Gas Release in Metallic Nuclear Fuels,” CEA-R-3888 (1969).
- [Lahm 1993] C. E. Lahm, J. F. Koenig, R. G. Pahl, D. L. Porter, D. C. Crawford, “Experience with advanced driver fuels in EBR-II,” J. Nuclear Materials 204 (1993).
- [Leggett 1993] R.D. Leggett, L.C. Walters, “Status of LMR fuel development in the United States of America.” J. Nuclear Materials 204 (1993).
- [Leppanen 2015] J. Leppanen, et al., “The Serpent Monte Carlo code: Status,

- development and applications in 2013,” *Annals of Nuclear Energy* 82, 142-150 (2015).
- [Miao 2019] Y. Miao, et al., “Fuel performance evaluation of anular metallic fuels for an advanced fast reactor,” *Nuclear Engineering and Design* 352, 110157 (2019).
- [Mikityuk 2017] K. Mikityuk, et al., “ESFR-SMART: new Horizon-2020 project on SFR safety,” *Proc. of IAEA FR2017, Ekaterinburg, Russian Federation* (2017).
- [Miles 1988] K.J. Miles, *Proceedings of the International Topical Meeting in Safety of Next Generation Fast Reactors, 1–5 May, American Nuclear Society, La Grange Park, IL, Seattle, WA* (1988).
- [Nakamura, 2001] K. Nakamura, et al., “Reaction of Uranium-Plutonium Alloys with Iron,” *Journal of Nuclear Science and Technology*, Vol. 38, pp. 112-119, (2001).
- [Ogata 1999] T. Ogata, et al., “Development and validation of ALFUS: an irradiation behavior analysis code for metallic fast reactor fuels,” *Nuclear Technology* Vol. 128, pp. 113-123, (1999).
- [Ohta 2015] H. Ohta, et al., “Irradiation of minor actinide-bearing uranium-plutonium-zirconium alloys up to ~ 2.5 at.%, ~ 7 at.%, and ~ 10 at.% burnups,” *Nuclear Technology*, Vol. 190, pp. 36-51, (2015).
- [Olson 1980] N. J. Olson, C. M. Walter, W. N. Beck, *Nuclear Technology* 28 (1980).
- [Pahl 1991] R. G. Pahl, D. L. Porter, D. C. Crawford, L. C. Walters, “Irradiation Behavior of Metallic Fast Reactor Fuels,” ANL/CP-73323, Argonne National Laboratory (1991).
- [Pahl 1993] R. G. Pahl, et al., “Performance of HT9 Clad Metallic Fuel at High Temperature,” Vol. 204, pp. 141-147, *Journal of Nuclear Materials*, (1993).
- [Porter 1986] D. L. Porter, G. L. Hofman, B. R. Seidel, L. C. Walters, “Factors Controlling Metal Fuel Lifetime,” *Proceedings of the International Conference on Reliable Fuels for Liquid Metal Reactors, Tucson, AZ* (1986).
- [Pusa 2010] M. Pusa and J. Leppanen, “Computing the Matrix Exponential in Burnup Calculations,” *Nuclear Science and Technology*, 164(2), 140-150 (2010).
- [Rineiski 2018] A. Rineiski, et al., “Specifications of the new core safety measures,” ESFR-SMART Deliverable D1.2, 2018.
- [Rineiski 2022] A. Rineiski, et al., “ESFR-SMART core safety measure and their preliminary assessment,” *J. Nuclear Engineering and Radiation Science*, Vol. 8(1), 011322 (2022).
- [Seidel 1977] B. R. Seidel, R. E. Einziger, “In-Reactor Cladding Breach of EBR-II Driver Fuel Elements,” *International Conference on Radiation Effects in Breeder Reactor Structural Materials, AZ* (1977).
- [Seidel 1983] B. R. Seidel, E. K. Hemsley, “High-Ramp-Rate Transient Performance of EBR-II Metallic Driver Fuel,” *ANS Transactions, CONF-841-47-43* (1983).
- [Seidel 1984] B. R. Seidel, L. C. Walters, “Performance of Metallic Fuels in Liquid-Metal Fast Reactors,” *ANS Transactions, CONF-841109-2* (1984).
- [Seidel 1986(a)] B. R. Seidel, D. L. Porter, L. C. Walters, “Experience with EBR-II Driver Fuel,” *Proceedings of the International Conference on Reliable Fuels for Liquid Metal Reactors, Tucson, AZ* (1986).
- [Seidel 1986(b)] B. R. Seidel, G. L. Batte, C. E. Lahm, R. M. Fryer, J. F. Koenig, “Off-Normal Performance of EBR-II Driver Fuel,” *Proceedings of the International Conference on Reliable Fuels for Liquid Metal Reactors, Tucson, AZ* (1986).
- [Seidel 1987] B. R. Seidel, L. C. Walters and Y. I. Chang, “Advances in Metallic Nuclear Fuel,” *J. Metals*, 39 (1987).
- [Seidel 1990] B. R. Seidel, G. L. Batte, N. E. Dodds, C. E. Lahm, G. L. Pahl, “Recent Progress in the Development of Metallic Fuel,” *International Topical meeting on the Safety, Status and Future of Commercial Reactor and Irradiation*

- Facilities, Idaho (1990).
- [Sofu 1996] T. Sofu, J. M. Kramer, J. E. Cahalan, Nuclear Technology 113 (1996).
- [Sridharan 2012] K. Sridharan, et al., "Development of Diffusion Barrier Coating and Deposition Technologies for Mitigating Fuel Cladding Chemical Interactions," NEUP-09-779, University of Wisconsin Madison (2012).
- [Stevenson 1987] C. E. Stevenson, "The EBR-II Fuel Cycle Story," American Nuclear Society (1987).
- [Till 1988] C. E. Till and Y. I. Chang, "The Integral Fast Reactor," Advances in Nuclear Science and Technology, 20 (1988).
- [Tsai 1991] H. Tsai, "Behavior of Low-Burnup Metallic Fuel Pins at Elevated Temperatures," International Fast Reactor Safety Meeting II, Utah (1991).
- [Wade 1989] D. C. Wade, E. K. Fujita, "Trends versus Reactor Size of Passive Reactivity Shutdown and Control Performance," Nucl. Sci. Eng. 103, 182 (1989).
- [Waltar 2012] A.E. Waltar, D.R. Todd, P.V. Tsvetkov, Fast Spectrum Reactors, Springer, 2012.
- [Walters 1980] L. C. Walters, J. H. Kittel, Nuclear Technology 48 (1980)
- [Walters 1984] L. C. Walters, B. R. Seidel, J. H. Kittel, "Performance of Metallic Fuels and Blankets in Liquid-metal Fast Breeder Reactors," Nuclear Technology 65 (1984).
- [Walters 1987] L. C. Walters, "Metallic Fuel Development," US/USSR Specialist Meeting in Fast Reactor Core Components, Richland, Washington, September 8-11 (1987).
- [Walters 1999] L.C. Walters, "Thirty years of fuels and materials information from EBR-II," J. Nuclear Materials 270 (1999).
- [Walters 2000] L.C. Walters, "Nuclear Fuel Considerations for the 21st Century," Progress in Nuclear Energy, Vol. 40 (2002).
- [Wright 2010] A. Wright, et al., "Advanced Metallic Fuel Concept for Reliable Performance to Ultra-high Burnup," Transaction of the American Nuclear Society, Vol. 106 (2012).
- [Zhang 2016] Y. Zhang and K. Mikityuk, "Static and transient analysis of a medium-sized sodium cooled fast reactor loaded with oxide, nitride, carbide and metallic fuels," Annals of Nuclear Energy 87, 761-771 (2016).